THIRD SEMI-ANNUAL TECHNICAL REPORT

Contract DAHC15-70-C-0187

RESEARCH ON THE PROPERTIES OF AMORPHOUS SEMICONDUCTORS AT HIGH TEMPERATURES

Prepared by: Energy Conversion Devices, Inc.
1675 W. Maple Road
Troy, Michigan 48084

For: Advanced Research Projects Agency
[Order No. 1570; Program Code 0D10]

Contract Period: 18 May 1970 to 18 May 1972

Total Contract Price: $791,352

J. P. deNeufville
Program Technical Manager
313-549-7300

S. C. Moss
Director, Science Department

Copy No. 14

Unclassified

Security Classification

DOCUMENT CONTROL DATA - R&D

(Security classification of title, body of abstract and indexing annotation must be entered when the overall report is classified)

1. ORIGINATING ACTIVITY (Corporate author) Energy Conversion Devices, Inc. 1675 W. Maple Road, Troy, Michigan 48084	2a. REPORT SECURITY CLASSIFICATION Unclassified 2b. GROUP N/A

3. REPORT TITLE

RESEARCH ON THE PROPERTIES OF AMORPHOUS SEMICONDUCTORS AT HIGH TEMPERATURES

4. DESCRIPTIVE NOTES (Type of report and inclusive dates)

Third Semi-Annual Technical Report - 18 May 1971 through 18 December 1971

5. AUTHOR(S) (Last name, first name, initial)

John P. deNeufville

6. REPORT DATE	7a. TOTAL NO. OF PAGES	7b. NO. OF REFS
18 May 1972	83	30

8a. CONTRACT OR GRANT NO.	9a. ORIGINATOR'S REPORT NUMBER(S)
DAHC15-70-C-0187 b. PROJECT NO. 1001/36 c. d.	516-3 9b. OTHER REPORT NO(S) (Any other numbers that may be assigned this report) None

10 AVAILABILITY/LIMITATION NOTICES

The distribution of this report is unlimited.

11 SUPPLEMENTARY NOTES	12. SPONSORING MILITARY ACTIVITY
	Advanced Research Projects Agency Arlington, Virginia 22209

13 ABSTRACT

A summary of the major accomplishments described in this report is as follows:

1. The demonstration of argon effusion kinetics versus temperature as a useful monitor of diffusional processes in chalcogenide glasses as well as a sensitive probe of argon content.
2. The association of trapped or reacted oxygen in sputtered amorphous silicon and germanium with a compressed structure resulting from the formation of Si-O-Si and Ge-O-Ge bonds. This oxidation also influences other properties and, in germanium, is shown to anneal out through phase separation.
3. The elucidation of the excellent epitaxy of Pd_2Si on silicon that permits the formation of a single crystal silicide during the room temperature deposition of Pd over (111) Si.
4. The discovery of simple instability criteria that lead to filament formation in S shaped negative differential conductivity (SNDC) devices.
5. The systematic description of crystallization phenomena in Ge-Te glasses associated with memory behavior. Consistent with the T_g behavior and with the thermodynamic results, glasses richer in Te than $GeTe_2$ first crystallize Te in a Ge enriched matrix via a nucleation and growth process in an, initially, single phase homogeneous glass. Between GeTe and a $GeTe_2$ phase separation appears to take place with GeTe crystallization preceding the eventual crystallization of

(continued on reverse)

DD FORM 1 JAN 64 1473

Unclassified

Security Classification

14. KEY WORDS	LINK A		LINK B		LINK C	
	ROLE	WT	ROLE	WT	ROLE	WT
Amorphous Semiconductors						
Amorphous Materials						
Chalcogenide Materials						
High temperature device materials						

the Te enriched glass ($GeTe_2$) into Te and GeTe.

6. The measurement of compositionally dependent heats of crystallization and defect annealing for sputtered amorphous Ge-Te films leading to the identification of two ordered amorphous structures: $GeTe_2$ and GeTe. The ordering at $GeTe_2$ supports the random network SiO_2 structural model for this composition, whereas the ordering at GeTe suggests a 3-fold coordinated structural model for this composition. Between $GeTe_2$ and GeTe we have found thermodynamic and structural evidence for phase separation into these ordered structures.

7. The refinement of the structure of Ge-Te glasses based on the combined neutron and X-ray radial density analyses.

8. The analysis of optical absorption, dc conductivity and thermopower results for $GeTe_2$ - $GeSe_2$ alloys leading to a band structure model for these amorphous phases in their virgin state after sputtering, and in their annealed state after heating to the vicinity of T_g. The effect of annealing the $GeSe_2$-rich films is to move the Fermi level across the center of the gap, producing a rapid transition from p-type to n-type conduction.

9. The development, in conjunction with R. Bube and T. Arnoldussen of Stanford University, of a method for analysis of photoconductivity results which places strong constrainst on the allowable density of states.

10. The application of this photoconductivity analysis to determine the effect of annealing upon the band structure of sputtered amorphous $GeTe_2$. Preliminary results indicate that the tailing of the valence band states into the gap increases with annealing, but that the relative increase in the valence band tail width is only about half the relative increase in the gap width.

11. The extension of the 3-fold coordination model leading to the discovery of new high T_g glasses in the GeTe - SiTe - As and GeAsSe - GeAsTe systems. Combining these results with the results described in Item 7 above for Ge-Te alloys, leads us to speculate on the possibility of widespread 3-fold coordination for chalcogenide alloys whose average valence electron number is 5 per atom. This coordination, which could result from a partial electron transfer from the chalcogenide component to the Group IV component, would lead to enhanced ionic bonding and higher values of T_g.

12. A new discussion of ac conductivity data written in order to clarity conflicting interpretations of these experiments in the determination of the density of states function of amorphous semiconductors.

TABLE OF CONTENTS

		Page
1.	Introduction and Summary of Major Accomplishments	1
	1.1 Introduction	1
	1.2 Summary of Major Accomplishments	2
2.	Survey of Thermodynamic, Structural, Optical and Electrical Transport Properties in Prototypical Glassy Chalcogenide Systems	4
	2.1 Introduction	4
	2.2 Ge-Te System	7
	2.2.1 Review of Thermodynamics and Glass-forming Tendencies: Structural Models	7
	2.2.2 Thermodynamic Data for Ge-Te Alloys	10
	2.2.3 Conductivity of Amorphous Ge-Te Films	19
	2.2.4 Crystallization Behavior of Amorphous Ge-Te Films	23
	2.2.4 Thermally Stimulated Argon Effusion From Sputtered $GeTe_2$	33
	2.2.6 Conclusions Regarding Atomic Structure of Amorphous Ge-Te Alloys	37
	2.3 Sputtered Amorphous $GeTe_2$ - $GeSe_2$ Alloys: New Transport Measurements and Proposed Band Model	40
	2.3.1 Introduction	40
	2.3.2 Photoconductivity of $GeTe_2$	40
	2.3.3 Thermoelectric Power of $GeTe_2$ - $GeSe_2$ Alloys	42
	2.3.4 A Band Level Picture of $GeTe_2$ - $GeSe_2$ Films: The Effect of Annealing	54
	2.4 Survey Studies of High T_g Ternary and Pseudo-Ternary Chalcogenide Systems	60
	2.4.1 Introduction	60
	2.4.2 Experimental Results	63
	2.4.3 Conclusions	64
3.	Abstracts of Completed Work	69
	3.1 Introduction	69

Table of Contents – cont'd.

		Page
	3.2 Structural Studies	70
	3.3 Thermal Analysis of Materials	73
	3.4 Theoretical Studies in Transport and Switching	74
4.	List of Contributors	76
5.	References	78
	Appendix I	80
	Appendix II	81
	Appendix III	82

1. INTRODUCTION AND SUMMARY OF MAJOR ACCOMPLISHMENTS

1.1 Introduction

The present technical report on ARPA contract DAHC15-70-C-0187 reviews the work performed under this contract from May 18, 1971 to December 18, 1971, although more recent results have also been included for topics which we are continuing to investigate. This is the third technical report in a two year study focused on amorphous semiconductors for high temperature applications. As this program nears its completion, an increasing large proportion of the work is becoming available in published form, primarily in the Journal of Non-Crystalline Solids, Materials Research Bulletin, Journal of Applied Physics, Solid State Communications and other similarly appropriate publications. For the first time in these technical reports, we have presented the completed work in abstract form in the main body of the report, and have appended the corresponding reprints and preprints separately. The extended sections of the text deal with several interdisciplinary survey studies of prototypical chalcogenide systems. In general each of these on-going survey studies will be published as a series of self-contained topics, so that the extended discussion in the present and preceeding reports is intended to provide an overall perspective of this work. Many of our ARPA investigations will, of course, appear as contributions to Vol. 8 - 10 of The Journal of Non-Crystalline Solids which is exclusively devoted to the recent Ann Arbor Conference on the Physics of Amorphous and Liquid Semiconductors. The research covered by these articles has largely been described in the preceeding reports to ARPA.

1.2 Summary of Major Accomplishments

1. The demonstration of argon effusion kinetics versus temperature as a useful monitor of diffusional processes in chalcogenide glasses as well as a sensitive probe of argon content.

2. The association of trapped or reacted oxygen in sputtered amorphous silicon and germanium with a compressed structure resulting from the formation of Si-O-Si and Ge-O-Ge bonds. This oxidation also influences other properties and, in germanium, is shown to anneal out through phase separation.

3. The elucidation of the excellent epitaxy of Pd_2Si on silicon that permits the formation of a single crystal silicide during the room temperature deposition of Pd over (111) Si.

4. The discovery of simple instability criteria that lead to filament formation in S shaped negative differential conductivity (SNDC) devices.

5. The systematic description of crystallization phenomena in Ge-Te glasses associated with memory behavior. Consistent with the T_g behavior and with the thermodynamic results, glasses richer in Te than $GeTe_2$ first crystallize Te in a Ge enriched matrix via a nuclueation and growth process in an, initially, single phase homogeneous glass. Between GeTe and a $GeTe_2$ phase separation appears to take place with GeTe crystallization preceding the eventual crystallization of the Te enriched glass ($GeTe_2$) into Te and GeTe.

6. The measurement of compositionally dependent heats of crystallization and defect annealing for sputtered amorphous Ge-Te films leading to the identification of two ordered amorphous structures: $GeTe_2$ and GeTe. The ordering at $GeTe_2$ supports the random network SiO_2 structural model for this composition, whereas the ordering at GeTe suggests a 3-fold coordinated structural model for this composition. Between $GeTe_2$ and GeTe we have found thermodynamic and structural evidence for phase separation into these two ordered structures.

7. The refinement of the structure of Ge-Te glasses based on the combined neutron and X-ray radial density analyses.

8. The analysis of optical absorption, dc conductivity and thermopower results for $GeTe_2$ - $GeSe_2$ alloys leading to a band structure model for these amorphous phases in their virgin state after sputtering, and in their annealed state after heating to the vicinity of T_g. The effect of annealing the $GeSe_2$-rich films is to move the Fermi level across the center of the gap, producing a rpaid transition from p-type to n-type conduction.

9. The development, in conjunction with R. Bube and T. Arnoldussen of Stanford University, of a method for analysis of photoconductivity results which places strong constraints on the allowable density of states.

10. The application of this photoconductivity analysis to determine the effect of annealing upon the band structure of sputtered amorphous $GeTe_2$. Preliminary results indicate that the tailing of the valence band states into the gap increases with annealing, but that the relative increase in the valence band tail width is only about half the relative increase in the gap width.

11. The extension of the 3-fold coordination model leading to the discovery of new high T_g glasses in the GeTe - SiTe - As and GeAsSe - GeAsTe systems. Combining these results with the results described in Item 7 above for Ge-Te alloys, leads us to speculate on the possibility of widespread 3-fold coordination for chalcogenide alloys whose average valence electron number is 5 per atom. This coordination, which could result from a partial electron transfer from the chalcogenide component to the Group IV component, would lead to enhanced ionic bonding and higher values of Tg.

12. A new discussion of ac conductivity data written in order to clarify conflicting interpretations of these experiments in the determination of the density of states function of amorphous semiconductors.

2. SURVEY OF THERMODYNAMIC, STRUCTURAL, OPTICAL AND ELECTRICAL TRANSPORT PROPERTIES IN PROTOTYPICAL GLASSY CHALCOGENIDE SYSTEMS.

2.1 Introduction

In the first and second technical reports under this contract we emphasized the importance of stoichiometry in determining the structural state and physical properties of chalcogenide glasses.[1,2] In contrast to random-covalent models, which require only valency satisfaction to account in a general way for all the electronic properties of chalcogenide glasses, we have shown that ordering effects produce most of the property singularities observed at specific chemical compositions, for bulk and well annealed thin film glasses.[3] These ordering effects in the Ge-Te binary result because the partially-ionic Ge-Te bond is stronger than the Ge-Ge and Te-Te bonds. The importance of these discoveries lies in the difficulty of studying such ordering effects via direct structural (PDF) methods even for binary systems. We have continued to utilize these ordering concepts in selecting model binary, ternary and quaternary systems for detailed analysis of electronic and thermodynamic properties.

The samples for these studies were produced by rf sputtering films of various thicknesses (0.3 - 20 μ), a technique which vastly simplifies the production of films of known composition with consistently reproducible properties. We rely primarily on the careful preparation of sputtering cathodes and on the translation of compositional fidelity from cathode to film to achieve films of specified compositions. The Ge-Te and Ge-Te-Se

systems appear to be especially well behaved in this regard, as we have verified by preliminary microprobe analysis. Arsenic, on the other hand, appears to be partially depleted during sputtering, possibly because of a lower "sticking coefficient", while thallium appears to be enriched. Survey studies of sputtered films in systems containing these components are therefore subject to greater compositional uncertainty and require closer microprobe monitoring.

We have utilized rf sputtering of thin films in order to widen the accessible compositional range of glass formation in prototypical systems beyond the limits achievable by almost any other method of sample preparation. Sputtered thin films differ from glasses prepared by the continuous solidification of a liquid in three respects. The first and inescapable consequence of sputtering is the incorporation of argon into the films. We have quantitatively characterized this effect in $GeTe_2$[4], a structurally simple material whose physical and thermodynamic properties have been extensively evaluated in current and previous portions of our high temperature chalcogenide materials research program.

A second consequence of sputtering is the incorporation of a substantial concentration of presently unspecified defects. The enthalpy of any glass below T_g always depends on its method of preparation and its annealing history. This central fact concerning the demonstrable instability of all real glasses has been the experimental platform upon which the theories of an ideal metastable glassy state have been built[5]. However the enthalpies of some sputtered amorphous alloys display very large departures

from their annealed values. We have measured these departures for a series of Ge-Te amorphous alloys in order to correlate the magnitude of the observed heat of annealing with, say, the separation of the deposition temperature from T_g, the glass transition temperature. We have observed significant optical and transport property changes occurring on the same time scale and within the same temperature range as the exothermic annealing of defects, and these property changes seem clearly attributable to the removal of the defects. Such measurements include the photoconductivity of $GeTe_2$ and the dc conductivity and thermopower of selected alloys in the Ge-Te binary and the $GeTe_2$ - $GeSe_2$ pseudobinary systems. On the other hand, we have observed that the magnitude and temperature dependence of the thermally stimulated argon effusion is not simply correlated (and therefore appears to be unrelated) with these thermal and electronic property changes introduced by annealing below the crystallization or glass transition temperature. Thus a microscopic description of these defects has not been achieved.

The third consequence of the sputtering of amorphous films is often the apparent loss of the thermal manifestation of T_g or, in effect, the replacement of a T_g endotherm by a crystallization or phase separation exotherm for compositions which are far removed from regions of bulk glass formation. This phenomenon has often been described, for example, for all forms of amorphous Ge and Si[6], for evaporated GeO_x alloys[7] and for the high Ge-content sputtered alloys in the Ge-Te system[8]. We have confirmed the existence of this effect in Ge-Te sputtered amorphous

alloys and have found that the transitional composition lies at or near $GeTe_2$, in the same composition range wherein other structural and thermodynamic changes occur. We propose a tentative model for the origin of this effect.

2.2 Ge-Te System

2.2.1 Review of Thermodynamics and Glass-forming Tendencies. Structural Models.

We have undertaken a comprehensive study of amorphous Ge-Te thin films prepared by rf sputtering. We selected this system not only because alloys based on $Ge_{85}Te_{15}$ display highly reversible memory switching, but also because it provides an opportunity to examine a variety of structural prototypes and to correlate in detail the transport, optical and thermodynamic properties of these structures. Much of this work has focused on the role of annealing effects, i.e., the irreversible removal, upon heating, of structural and chemical (i.e., argon entrapment) defects which were incorporated into the films during their deposition.

In the course of these experiments we have attempted to define and quantify the role of composition in controlling the structural state and physical properties of a series of glass alloys in a binary system. Our motivation for such a study lay in the then current state of our understanding of these materials:

1. We had already observed a T_g maximum and had qualitative indication of a resistivity maximum in the vicinity of $GeTe_2$[3].

Sputtered amorphous $GeTe_2$ has been studied extensively (see Section 2.3) and the role of stoichiometry on its properties posed a significant challenge to our understanding of structure-property relationships in a chalcogenide glass system.

2. We had measured an order-disorder transition in Te-rich binary liquids at about 400°C whose energy suggested a high degree of local order for lower temperature liquids and glasses[3].

3. Extensive X-ray diffraction data were available[9] which, while in agreement with the random covalent model of Mott, could not distinguish between an ordered versus a disordered covalent network, or even between a network containing 3-fold Ge and Te versus a network containing only 4-fold Ge and 2-fold Te.

4. The existence of phase separation in this system, while in our view[2,3] apparently absent between Te and $GeTe_2$, had neither been confirmed or rejected for the higher Ge content glasses.

5. A controversy existed in the literature concerning the short range order in amorphous GeTe[10]: If Ge and Te are each in 3-fold coordination, singularities in thermodynamic, optical and transport properties might be expected at the stiochiometric GeTe composition. In contrast, if Ge remains 4-fold and Te remains 2-fold between $GeTe_2$ and Ge, then no property singularities would be anticipated at the stoichiometric

GeTe composition.

6. A large discrepancy existed in the reported crystallization temperature of amorphous sputtered[11,12] and evaporated[13] GeTe, which heightened the uncertainty concerning the existence of a stoichiometric structural prototype corresponding to amorphous GeTe.

7. Structural models for $GeTe_2$[3] and Ge[14] have been proposed and in the case of Ge[15] have received some detailed experimental confirmation. We wanted to accumulate additional data to test the proposed $GeTe_2$ structural model and to decide whether a stoichiometric (i.e., ordered 3-fold coordination) model could also be proposed on the basis of the existence of property singularities at the GeTe composition.

The results of this experimental program are still incomplete, but many significant features have emerged. The observations can be classified into:

1. Thermodynamic data, including measurements of density, T_g, T_x, heat of defect annealing and heat of crystallization vs. composition.

2. Transport data, especially measurements of dc conductivity vs. temperature and composition before and after defect annealing. (Measurements of thermopower and optical absorption of thin films are currently in progress, and will

be reported in the final technical report).

3. Crystallization data, including the effect of film composition on nucleation rates and crystallization products vs. temperature.

4. Thermally stimulated argon effusion from sputtered $GeTe_2$.

2.2.2 Thermodynamic Data for Ge-Te Alloys

We have measured, in a Perkin-Elmer DSC 1B scanning calorimeter, the enthalpies of crystallization and of defect annealing vs. composition for sputtered Ge-Te films containing 10 - 60% Ge. In addition we have measured the compositional dependence of the density of sputtered amorphous Ge-Te films. The defect annealing experiments provide information regarding the total defect energy and the kinetics of defect removal. The heats of crystallization reveal the energy difference between the amorphous and the fully crystallized forms of the Ge-Te alloys. These heats can be normalized to provide heat of formation data for the amorphous Ge-Te phase, thereby identifying regions of ordering and regions of clustering within this system. The density data have been obtained in order to confirm these ordering and clustering tendencies.

2.2.2.1 Heat of Defect Annealing

Because the optical and transport properties of sputtered glassy films are greatly affected by annealing below their crystallization temperatures, we have attempted to measure the energy differences between annealed and unannealed films. We noted in our preceeding

Figure 2.1 Enthalpy change occurring during defect annealing (▪) and crystallization (o) of sputtered amorphous Ge-Te films versus composition.

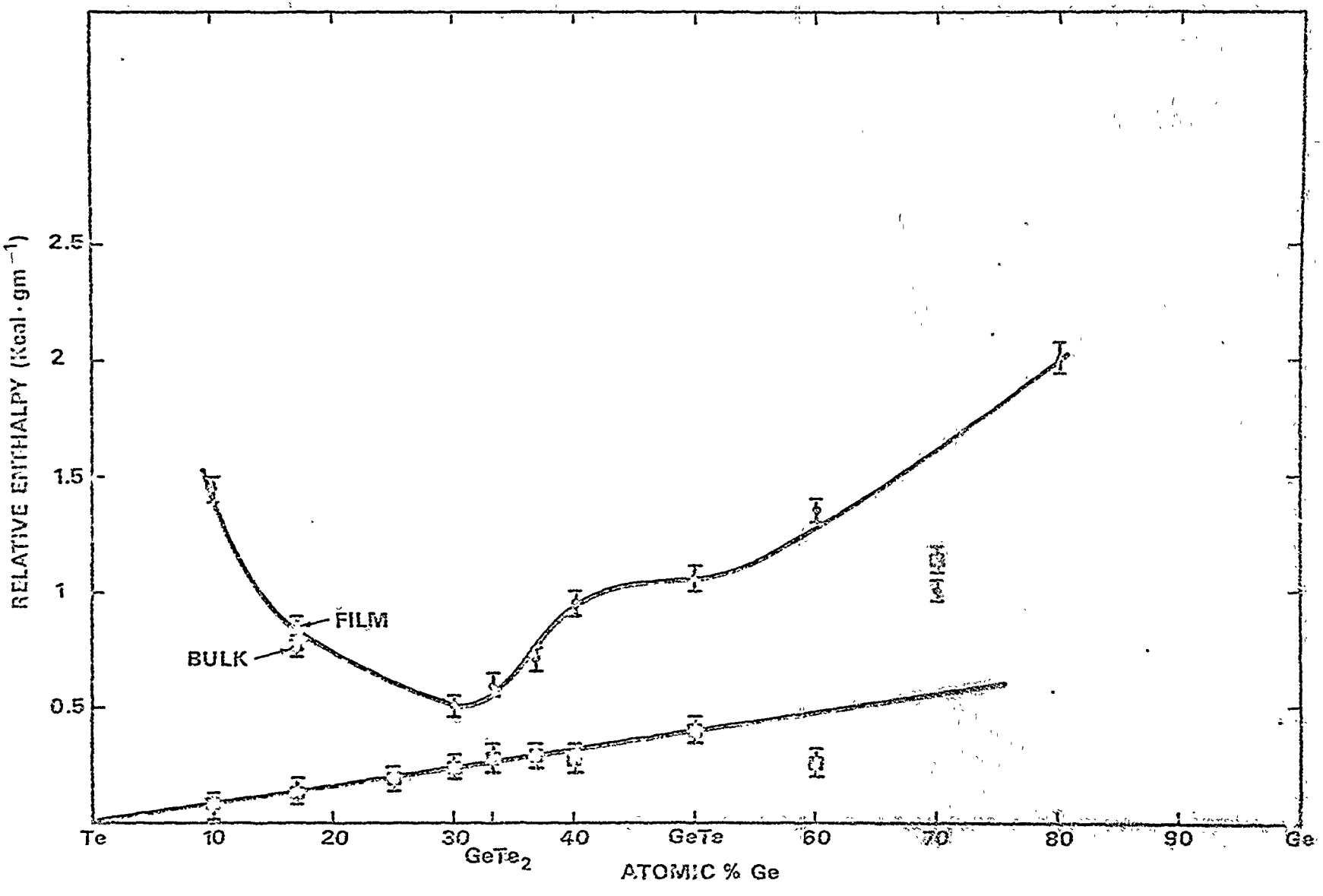
RELATIVE ENTHALPY (Kcal · gm⁻¹)
2.5
2
1.5
1
0.5
FILM
BULK
Te
10
20
30
GeTe2
40
GeTe
60
70
80
90
Ge
ATOMIC % Ge

II-A

technical report the qualitative observation of an exothermic effect accompanying the initial scanning of sputtered film samples from 25°C to T_g, as detected by careful comparison of the initial calorimeter scan trace and the rescanned trace. Since the optical and transport property annealing effects vary with film composition in a complicated way, we measured the compositional dependence of the stored energy (i.e., defect annealing energy) in the Ge-Te system. The data are plotted as squares in Figure 2.1. A roughly linear increase in stored energy with increasing Ge content is observed.

This result, in itself, suggests that the annealing process removes defects which bear no special relationship to stoichiometry. For example, there is no significant maximum in ΔH_{anneal} at $GeTe_2$, as one might expect if the high degree of chemical ordering of $GeTe_2$, inferred from the transport and optical properties of fully annealed glassy $GeTe_2$, were significantly enhanced by annealing. It thus appears that these defects are physical (i.e., vacancies, dangling bonds, unpaired valence electrons, distorted bonds, etc.) rather than chemical (i.e., a nonequilibrium distribution of bond types). If so, then the defect concentration should scale inversely with the self annealing which can occur during deposition, which in turn might scale with the departure of the deposition temperature from T_g or T_x. Indeed this is roughly correct: The increase in stored energy with increasing Ge tends to scale with the increasing differential between the deposition temperature and T_x (See section 2.2.3). We rule

out the release of trapped argon as a significant contribution to the defect annealing exotherm, because defect annealing occurs in a temperature range where less than 1% of the trapped argon is effused upon heating.

2.2.2.2 Heat of Crystallization

We have measured the heat of crystallization of amorphous Ge-Te alloys from $Ge_{10}Te_{90}$ to $Ge_{70}Te_{30}$ in the scanning calorimeter. The data were obtained using a 20 deg min^{-1} scanning rate, which produced a single crystallization exotherm for each composition for Ge contents up to $Ge_{40}Te_{60}$. Films containing more than 40 atomic percent Ge crystallized in two or more exothermic stages. For $Ge_{10}Te_{90}$ through $GeTe_2$, the crystallization exotherm was always preceeded by a T_g endotherm, which served as a convenient marker for distinguishing the exothermic effects of defect annealing below T_g from the exothermic effects of crystallization (above T_g). For the higher Ge content films, such a natural division is unavailable, and indeed the two exothermic effects tend to overlap to some extent. We have relied on X-ray diffraction evidence and on the large rate of increase of the exothermic effect accompanying the initial stages of crystallization to separate the observed combined exotherm into a defect annealing term and a crystallization term.

The data so obtained are plotted vs. composition in the upper

curve (full circles) in Figure 2.1. Minima in $\Delta H_x(X)$ occur near $Ge_{32}Te_{68}$ and $Ge_{50}Te_{50}$. These features are more evident when the measured heats of crystallization are referred to an absolute enthalpy scale (as in Figure 2.2) by evaluating $\Delta H_o(X)$, the 25°C heat of formation of the annealed amorphous alloys at 25°C versus composition. For this calculation we have taken the heat of formation of GeTe at 25°C as 4 k cal (gm atom)$^{-1}$ (30) and assumed that the fully crystallized films contain mixtures of GeTe crystals and Te crystals (if Te > 50 atomic percent) or Ge crystals (if Ge > 50 atomic percent). Thus the straight lines connecting the Te and Ge heats of formation (both zero by definition) to the GeTe heat of formation define the heat of formation of mixtures of either pair of crystals. To these values are added the measured heats of crystallization to obtain the calculated heats of formation of the amorphous alloys.

In this representation in Figure 2.2, the relevance of the heat of crystallization to the chemical ordering tendencies in these glasses becomes obvious. The lowest energy amorphous phase in the Ge-Te system occurs at the same composition, $Ge_{50}Te_{50}$, as the lowest energy crystalline phase. Another minimum appears at ~ $Ge_{33}Te_{67}$, i.e., near $GeTe_2$, displaced slightly to higher Ge than the minimum in Figure 2.1. The region of negative curvature in $\Delta H_o(X)$ which appears between these minima in Figure 2.2 should lead to phase separation if it leads to regions of negative curvature in the Gibbs free energy.

Figure 2.2 Enthalpy of formation at 25°C of crystalline and sputtered amorphous phases in the Ge-Te system versus composition. Enthalpy of formation of crystalline GeTe at 25°C from reference 30.

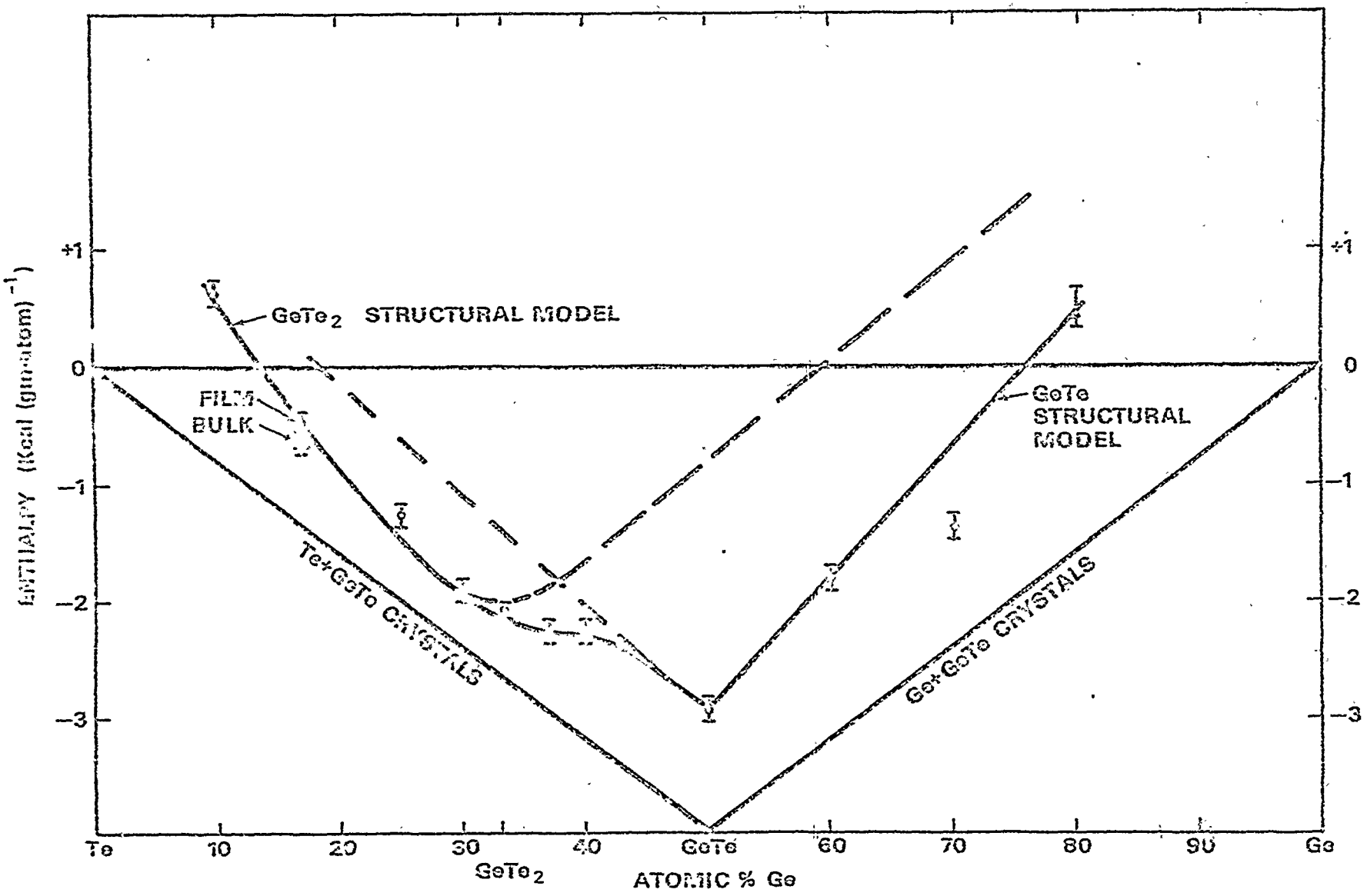
GeTe2 STRUCTURAL MODEL
FILM
BULK
GeTe
STRUCTURAL
MODEL
Te+GeTe CRYSTALS
Ge+GeTe CRYSTALS
+1
0
−1
−2
−3
Te
10
20
30
40
GeTe
60
70
80
90
Ge
GeTe2
ATOMIC % Ge

IS-4

We have obtained preliminary transmission electron microscope results which indicate the existence of phase separation prior to crystallization for the alloy $Ge_{40}Te_{60}$, i.e., near the point of maximum negative curvature in the $\Delta H_o(X)$ plot.

We draw the enthalpy minima in Figure 2.2 as continuous curves. A simple model for the minima at $GeTe_2$ and GeTe can be based on a large ordering tendency at these compositions. At $GeTe_2$, we assume that Ge is 4-fold and Te is 2-fold coordinated, and that only Ge-Te bonds are allowed. Addition of Te to this structure introduces weaker Te-Te bonds, while addition of Ge introduces weaker Ge-Ge bonds. The concentration of these excess bonds depends linearly on the concentration of excess Ge or Te, so the energy (enthalpy) of the glass structure would depend only on the relative bond concentrations. The extrapolations of this model to pure Te and pure Ge lead to the observed two-fold and four-fold coordinations observed for those glasses. No account is taken in this model for clustering or ordering tendencies among the excess Ge-Ge or Te-Te bonds. Small departures from complete ordering at GeTe would lead to the smooth $\Delta H_o(X)$ curve which best fits our data.

At GeTe we assume that the bonding effects which produce the energy minimum for the crystalline phase must exist for the amorphous phase as well. X-ray diffraction data[9] rule out the existence of the crystalline short range order in the glass. This structure is a rhombohedral distortion of the 6-fold NaCl structure,

yielding 3 near and 3 slightly less near neighbors of Ge in the first coordination shell of each Te, and vice-versa. A further distortion, resulting in only 3 unlike neighbors in the first coordination shell (i.e., a 3-fold structure) is consistent with the diffraction data, and would retain most of the ionic stabilization which is essential for a low energy (i.e., ordered) amorphous GeTe phase. Addition of Te or Ge to such a structure presumably results in the introduction of some 2-fold Te or 4-fold Ge sites, inasmuch as the postulated 3-fold structure can exist only in local environments which contain equal concentrations of Ge and Te. Again, the addition of either atom in excess of stoichiometry results in an introduction of weaker bonds, whose concentration depends linearly on the composition. And, again, the energy of the structure ought to vary linearly with this excess energy and thus with composition. The extrapolation of these linear regions to pure Ge and pure Te should coincide with the extrapolations of the $GeTe_2$ structure, in that both models treat the excess Ge-Ge and Te-Te bonds in the same way. Portions of these two extrapolations are shown as dashed lines in Figure 2.2.

2.2.2.3 Density of Sputtered Amorphous Ge-Te Alloys

We have measured the density of sputtered amorphous Ge-Te films by weighing a film of known thickness and area deposited on a thin cover glass slide. To improve the accuracy of the measurement we have measured the film thickness at 5 points on the 1" x 1"

Figure 2.3 Density of sputtered amorphous films in Ge-Te system versus composition.

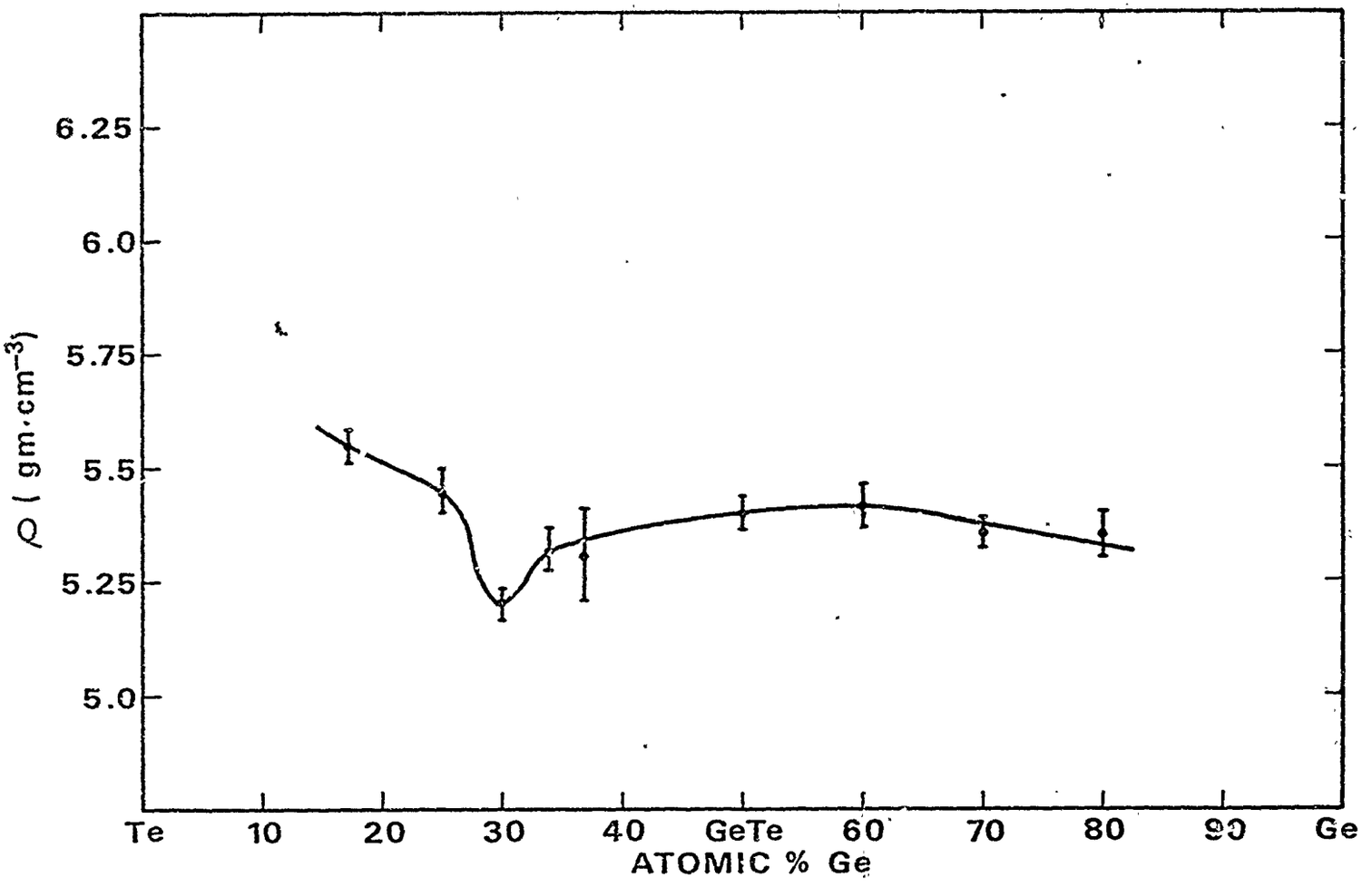
6.25
6.0
5.75
5.5
5.25
5.0
ρ (gm·cm⁻³)
Te
10
20
30
40
GeTe
60
70
80
90
Ge
ATOMIC % Ge

18-A

substrate and have run at least two replicate substrates for each data point. By these procedures we have reduced the errors of measurement substantially, and experimental scatter is approximately $\pm$ 1 - 2% in an average case.

The data so obtained are plotted in Figure 2.3 and reveal considerable structure. The density minimum in the vicinity of $GeTe_2$, seems to signify substantial departures from a random (ideal) solution behavior, and confirm indirectly the existence of an ordering tendency at the $GeTe_2$ composition. The density minimum near $GeTe_2$ coincides with the enthalpy minimum observed near the same composition. The approximate correspondence of the density and enthalpy minima seems in good accord with a fairly open structure for the fully cross-linked chalcogen saturated composition $GeTe_2$.

A word of caution regarding these density data must be made: while good agreement is observed between bulk and film densities at $Ge_{17}Te_{83}$ and $Ge_{15}Te_{85}$, defects introduced into films of higher Ge content during deposition will tend to decrease their density below that of a defect-free glass. On the other hand, annealing does not remove this density deficit in the case of the $GeTe_2$ - $GeSe_2$ system[3], but rather increases it slightly. Thus an unknown, compositionally dependent, defect term must be added to these data to deduce the defect-free glass densities.

2.2.3 Conductivity of Amorphous Ge-Te Films

Measurements of conductivity and electrical activation energy in the Ge-Te system have been obtained on a series of ~ 1 μm

Figure 2.4 Electrical conductivity at 25°C versus composition for amorphous Ge_xTe_{1-x} virgin and annealed sputtered alloy films.

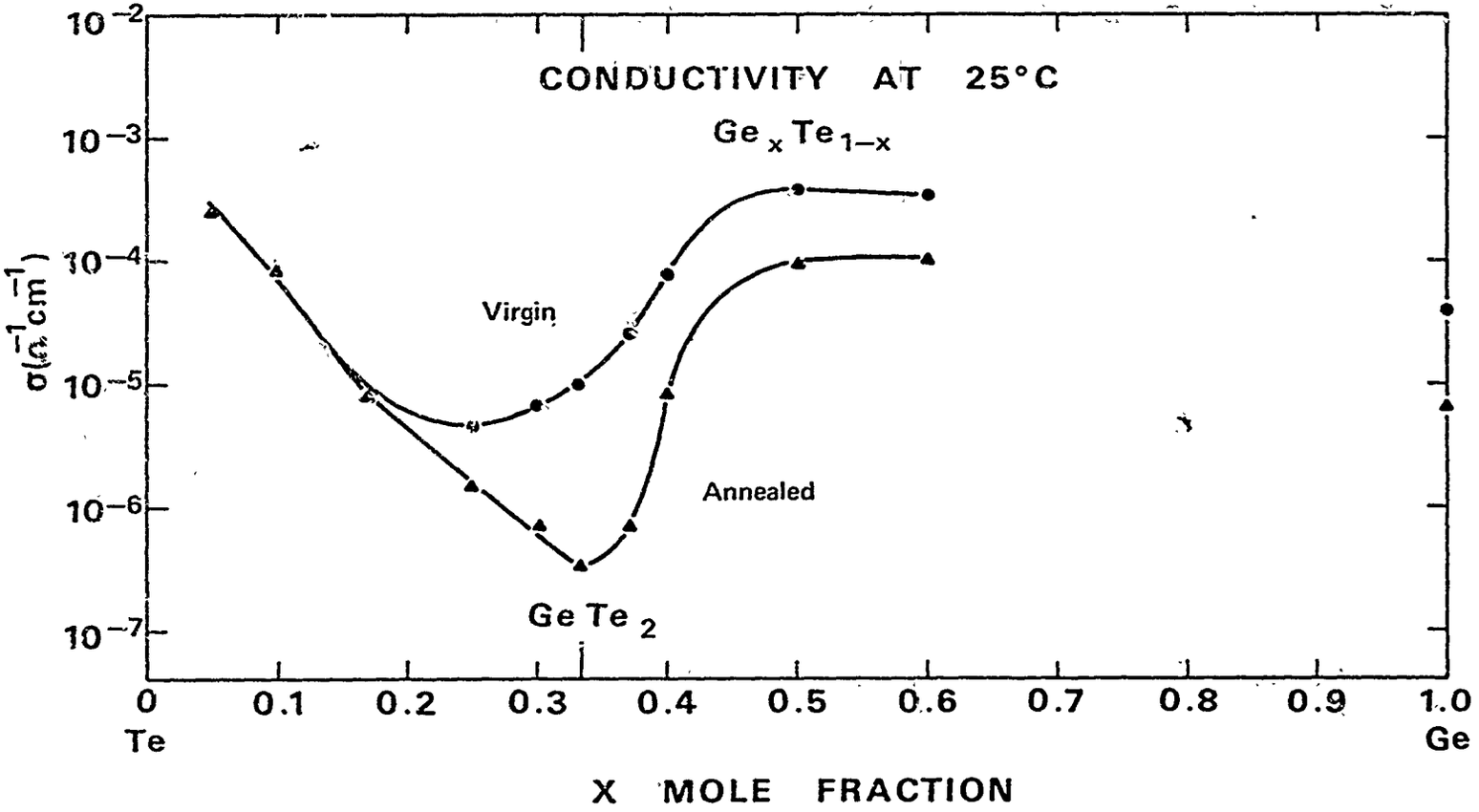
CONDUCTIVITY AT 25°C
Ge_xTe_{1-x}
Virgin
Annealed
$GeTe_2$
$\sigma(\Omega^{-1}cm^{-1})$
10^{-2}
10^{-3}
10^{-4}
10^{-5}
10^{-6}
10^{-7}
0
Te
0.1
0.2
0.3
0.4
0.5
0.6
0.7
0.8
0.9
1.0
Ge
X MOLE FRACTION

20-A

Figure 2.5 Conductivity activation energy at 25°C versus composition for amorphous $Ge_x Te_{1-x}$ virgin and annealed sputtered alloy films. Tangents of ln σ versus $10^3/kT$ at 25°C were used.

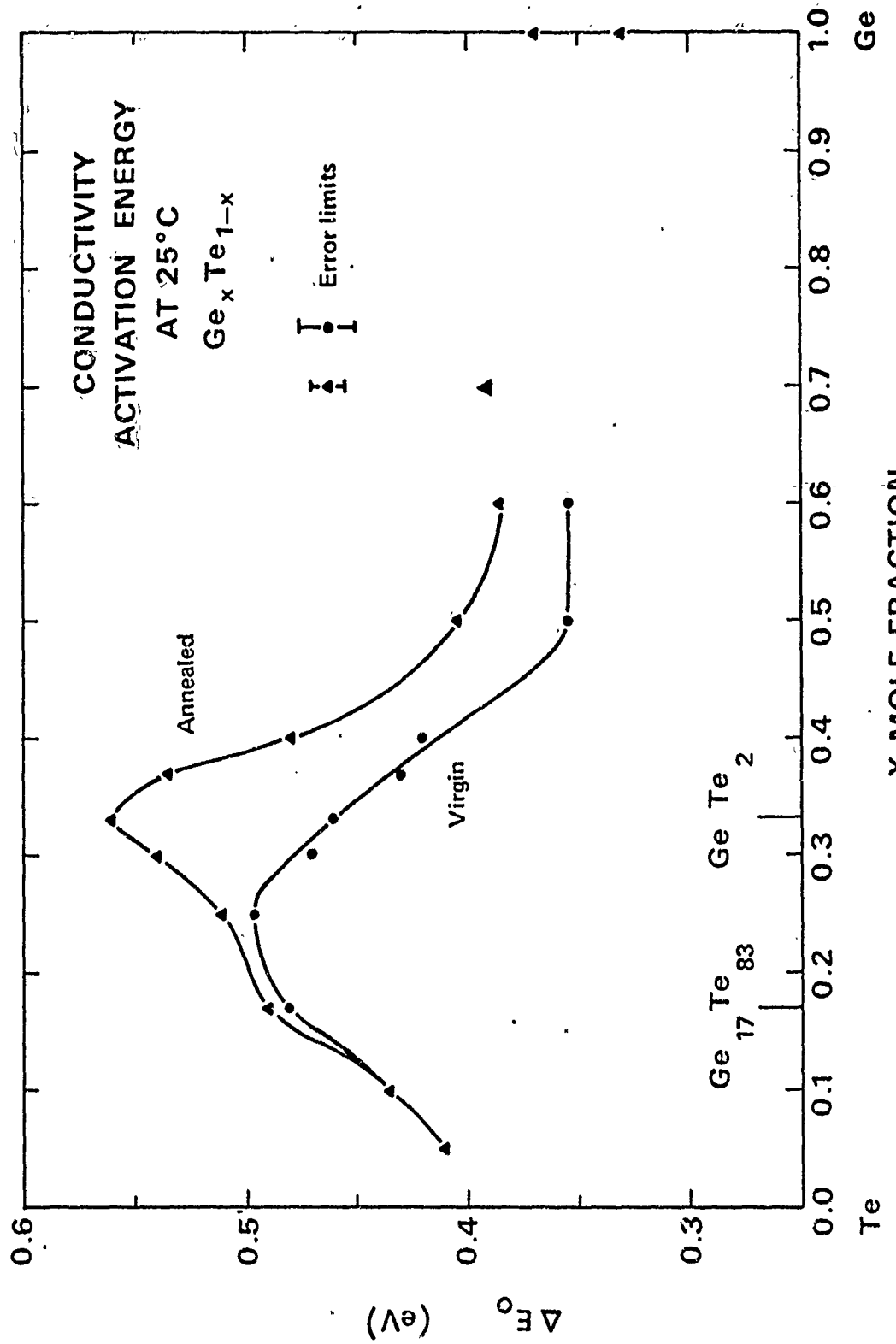
CONDUCTIVITY
ACTIVATION ENERGY
AT 25°C
Ge_xTe_{1-x}
Error limits
Annealed
Virgin
ΔE_o (eV)
0.6
0.5
0.4
0.3
0.0
0.1
0.2
0.3
0.4
0.5
0.6
0.7
0.8
0.9
1.0
Te
Ge
$Ge_{17}Te_{83}$
$GeTe_2$
X MOLE FRACTION

films sputtered onto electroded Al_2O_3 and Corning 7059 substrates. The typical experiment consisted of a heating cycle in high purity N_2 gas during which log i vs. T was measured at low fields ranging from 10^{-1} to 10^{-2} V cm^{-1}. By cycling the sample up and down in temperature the experimenter could usually observe the same three stages of conductivity behavior as described in section 2.3: low temperature virgin region, fully annealed region, fully crystallized region. We have emphasized the first two stages of this behavior, and have plotted in Figure 2.4 and 2.5 the 25°C values of conductivity and conductivity activation energy vs. composition for both virgin and annealed films. Both annealed curves show a pronounced singularity near $GeTe_2$. The virgin films show a broad activation energy maximum and conductivity minimum near the same composition but displaced a bit towards Te.

Clearly the chalcogen saturation structural model for $GeTe_2$ provides an attractive conceptual framework to account for the conductivity singularity found at $GeTe_2$ for the annealed films. In this view the introduction of excess Te or Ge to $GeTe_2$ requires the formation of new short range order configurations; some of the fully cross linked corner-sharing $GeTe_2$ tetrahedra must be perturbed to form some Ge-Ge or Te-Te linkages depending on the direction of departure from stoichiometry. The electronic states associated with these perturbed local configurations thus provide a mechanism

for lowering of the effective band gap relative to that of $GeTe_2$.

The effect of defects is to increase the conductivity and to smear out the conductivity and activation energy singularities observed for the annealed films at the $GeTe_2$ composition. Thus the largest annealing effect is to be found at $GeTe_2$, in contrast to the enthalpy data which indicate a monotonic increase of defects with Ge content assuming all defects have identical energies, Note that the annealed and virgin data asymptotically approach each other as the Te concentration is increased above 85 atomic percent. As the deposition temperature approaches the effective annealing temperature, the concentration of defects (excess enthalpy) in the virgin films approaches zero (i.e., the extrapolation to pure Te; see Figure 2.1).

The curves as presented are incomplete. We are extending these studies to include thermopower data and data on the Ge-rich portion of the system. At present we have no data to suggest any conductivity singularity at GeTe corresponding to the thermodynamic singularity. We anticipate that the comparison of conductivity, optical absorption and thermopower results will reveal any further singularities in the amorphous Ge-Te system, by analogy with our results for the $GeTe_2$-$GeSe_2$ system (see section 2.3).

2.2.4 Crystallization Behavior of Sputtered Amorphous Ge-Te Films

We have been able to sputter thin (~ 500 Å) amorphous films

of Te-Ge alloys over the range from 2.5% Ge to 100% Ge. The high Te cut-off for sputtering thick ($\geq 1\ \mu$) amorphous films in this system, for substrates held at $\sim 25^{o}C$, appears to be close to $Te_{95}Ge_5$. We have examined the thermal, electrical and structural manifestations of thermally induced crystallization in thick amorphous Ge-Te films, using calorimetry, dc conductivity and X-ray diffraction experiments. Additional structural data have been obtained on the thin films using electron diffraction and microscopy. Optical microscopic observations have also proved useful.

The goals of the thermal studies have been to observe the compositional dependence of T_g and T_x and to measure the heat released during crystallization. These samples were therefore heated relatively rapidly (20 deg min^{-1}) in order to obtain the maximum calorimetric sensitivity without introducing appreciable thermal lag. At this scanning rate crystallization of both Te and GeTe occurs in a single exotherm for alloys ranging in composition from $Ge_{10}Te_{90}$ to $Ge_{40}Te_{60}$. The temperature of this exotherm and its relationship to T_g as a function of composition is plotted in Figure 2.6.

Of the alloys reported in Figure 2.6, only amorphous GeTe shows two exotherms, an unsuspected result in view of the fact that it can crystallize to a single phase. X-ray analysis shows that the first exotherm yields the rhombohedral form of GeTe (i.e., the stable low temperature modification) and the second exotherm results in further GeTe crystallization accompanied by Ge crystallization. Thus

Figure 2.6 Glass transition temperature (o), beginning of crystallization exotherm (□) and peak of crystallization exotherm (△) of sputtered amorphous Ge-Te alloys heated at 20 deg. min. in a Perkin Elmer DSC-1B Scanning Calorimeter versus composition.

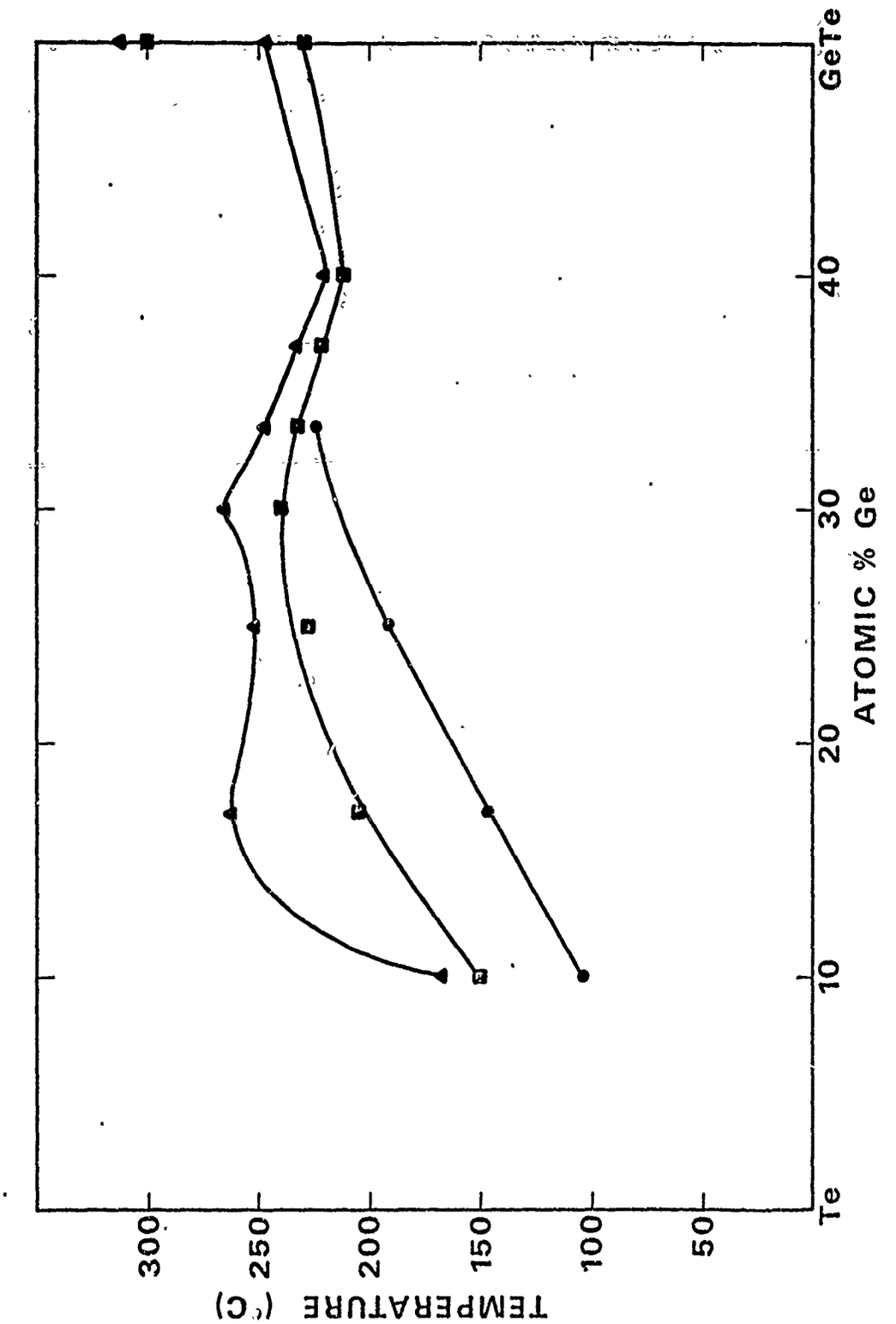
TEMPERATURE (°C)
300
250
200
150
100
50
Te
10
20
30
40
GeTe
ATOMIC % Ge

a departure from stoichiometry towards Ge appears to account for the discrepancy. We will obtain microprobe analysis to confirm this interpretation.

Note that $T_g(x)$ increases smoothly from $Ge_{10}Te_{90}$ to $GeTe_2$, beyond which no glass transition is observed. For higher Ge content films, crystallization occurs before any calorimetric manifestation of a glass transition. This observation is apparently independent of the rate of temperature increase up to 80 deg min^{-1}. While the absence of T_g in amorphous Ge[6] could be viewed[7] as an analogy to the thermal properties of glassy GeO_2 and SiO_2, whose structures can also be described as tetrahedrally coordinated random networks and which also lack any evidence of T_g, the abrupt cut-off of T_g in amorphous Ge-Te alloys near $GeTe_2$ appears to be a consequence of other factors. Rather than concluding that the fluidity transformation associated with T_g occurs without any thermal manifestation (e.g., the SiO_2 or GeO_2 case), we conclude that crystallization of amorphous Ge-Te alloys containing more than about 33% Ge occurs as a solid-solid transformation. In other words, the amorphous material technically devitrifies rather than undergoing a transition to the liquid state prior to crystallization. Indeed, the intersecting trends of T_g and T_x with increasing Ge content above $Ge_{30}Te_{70}$ seem to suggest that the T_g phenomena is experimentally inaccessible due to prior crystallization.

Normally such a transformation is ruled out[16] on kinetic

grounds; the atomic mobility required to produce measurable crystallization of the glass is not attained below T_g. However in the presence of suitable nucleating points (normally heterogeneous nuclei), atomic motion within the glass is not required; only motion of atoms at the glass-crystal interface is required. While the atomic mobility at this interface is normally equated with that of the bulk amorphous phase[16], either the presence of impurities or the existence of significant structural differences between the interface and the bulk amorphous phase can invalidate this assumption. The large differences in the crystallization temperatures reported for amorphous GeTe prepared by evaporation[13] and rf sputtering[12] may provide support for the role of impurities in catalyzing (or inhibiting) the devitrification transformation of amorphous GeTe. Alternatively, the motion of defects introduced during the deposition process may enhance the self-diffusion coefficients in the glass to the point where the atomic mobility is sufficient to allow crystallization. Again the nature and concentration of these defects (broken bonds, high energy SRO clusters, etc.) may depend sensitively on the deposition parameters of the film, independent of the impurity content.

In order to identify structural transformations associated with the progressive thermal crystallization of the amorphous Ge-Te alloys we annealed both non-electroded and electroded substrates in dry nitrogen, measuring in the first case the effect of annealing on the X-ray diffraction patterns, and in the second case the temperature

dependence of the dc conductivity. In these studies the annealing temperature was either held fixed (X-ray experiments) or changed slowly (ca. 3 deg min^{-1} in the conductivity experiments). These procedures, together with the thermal sinking provided by the substrates, assured that no appreciable self-heating of the films could accompany crystallization, resulting in a more detailed picture of the crystallization sequence than could be obtained by rapid scanning in the calorimeter.

Optical microscopy of partially crystallized films containing 25, 30, 33 and 50% Ge revealed the presence of spherulitic crystallites embedded in an amorphous matrix. These crystals appeared to nucleate heterogeneously at defect sites on the surface of the film, and ranged in concentration from 10^3 to 10^6 cm^{-2}. All the other films showed some sort of mottling on a sub-micron scale accompanying the early stages of crystallization, but the fine scale and the interfering effects of surface rumpling associated with the release of trapped argon inhibited detailed optical observations in these cases.

The most significant feature of the X-ray diffraction experiments was the identification of three crystallization regimes for amorphous Ge-Te alloys containing up to 50% Ge. The high Te regime, extending to 25% Ge, exhibits the two stage crystallization reported by Messier and Roy[12]. The first stage of crystallization begins just above T_g and involves the formation of fe crystals, while the second stage

of crystallization occurs at a uniform temperature of 230 $\pm$ 10°C and involves the formation of GeTe crystals accompanied by more Te[17]. As the Ge content approaches 30%, T_g approaches 220° or so, and the two crystallization events merge, resulting in the simultaneous crystallization of GeTe and Te in alloys containing 30 to 36% Ge. For higher Ge contents the third crystallization regime is encountered, in which GeTe becomes the initial crystallization product beginning at a progressively lower crystallization temperature as the Ge content is increased from 36 to 50%. For $Ge_{40}Te_{60}$, for example, GeTe begins to crystallize at ~ 180°C and crystallization of GeTe is joined at ~ 220°C by crystallization of Te. Simultaneous crystallization of GeTe and Te proceeds above 220°C.

These results, together with optical microscopy of the same films, suggest that the nucleation tendency of Te in amorphous Ge-Te alloys decreases with increasing Ge content, becoming negligible for Ge concentrations exceeding 33%, while the nucleating tendency of GeTe in amorphous Ge-Te alloys is negligible for Ge concentrations less than 33% and increases sharply with further Ge concentration. In the vicinity of $GeTe_2$, neither phase has a large nucleation rate, resulting in the observed very low nucleation density. Thus in order for a glass in the Te-rich regime to crystallize completely, it must become sufficiently enriched in Ge by tellurium crystallization to nucleate germanium telluride. Conversely, a glass in the Ge-rich regime (i.e., between $Ge_{36}Te_{64}$ and $Ge_{50}Te_{50}$) will initially

crystallize the telluride, rejecting Te into the residual amorphous phase until tellurium can nucleate. The compositional range in which both Te and GeTe can nucleate corresponds to the intermediate alloys (i.e., $Ge_{30}Te_{70}$ to $Ge_{36}Te_{64}$) which crystallize Te and GeTe simultaneously at about 230-240°C. This diffusion model for the observed nucleation barrier to second phase crystallization in the amorphous Ge-Te alloys accounts nicely for the observed constancy of second phase growth between 220 - 240°C for slow heating rates.

Some further comments on the compositional dependence of the Te and GeTe nucleation rates can be offered. Our structural model[3] for amorphous phases in the 0 - 33% Ge portion of the Ge-Te system involves a progressive elimination of Te-Te linkages with increasing Ge content. We cannot presently determine the spatial distribution of these Te chain segments. If they are clustered together, then such clusters obviously provide potential sites for the nucleation of Te crystals. Conversely, the high rate of GeTe nucleation in alloys containing more than 36% Ge may perhaps be taken as an indication that the short range order of crystalline GeTe exists, albeit in a distorted condition, in glassy alloys of similar composition. By this we imply that glasses near GeTe in composition may have 3-fold coordination rather than a mixture of 2-fold (Te) and 4-fold (Ge) corrdination. Finally, the relative difficulty of nucleating either GeTe or Te in the vicinity of GeTe, suggests, again

indirectly, the tetrahedrally coordinated random network structure model for this composition, which shares no common features with the SRO of either crystalline phase.

Dc conductivity was measured versus temperature for all the Ge-Te alloys as reported in section 2.2.3, and these measurements were extended into the temperature regime where thermally induced crystallization occurred. Two categories of crystallization effects were observed, corresponding more or less to the high nucleation rate regime (both Te-rich and Ge-rich) and the low nucleation rate regime. For high nucleation rates (i.e., very fine scale crystallization), progressive crystallization produced a gradual conductivity transition, resulting in departures from the intrinsic behavior usually observed prior to any crystallization. The resulting plots of log σ vs. $1/T$ at intermediate stages of crystallization cannot be simply analyzed, displaying a progressive flattening with increasing reciprocal temperature. Such a plot is shown for an analogous quaternary memory alloy, $Ge_{15}Te_{81}Sb_2S_2$, in Figure 2.7. However for low nucleation rate alloys such as $GeTe_2$, the initial stages of crystallization are barely detectable; the conductivity is shifted uniformly upward without change in activation energy. This process can continue for as many as two decades, at which point a 2 dimensional percolation path becomes established and the conductivity instantly jumps to the temperature independent level associated with the crystallized material ($\sim 10 \Omega^{-1} cm^{-1}$). An example of such behavior is shown in Figure 2.8.

Figure 2.7 Dc conductivity versus reciprocal temperature for a sputtered 1.2 μm thick film of $Te_{81}Ge_{15}Sb_2S_2$. 108°C 60 minute curve corresponds to amorphous film; annealing at successively higher temperatures caused successively more crystallization of tellurium.

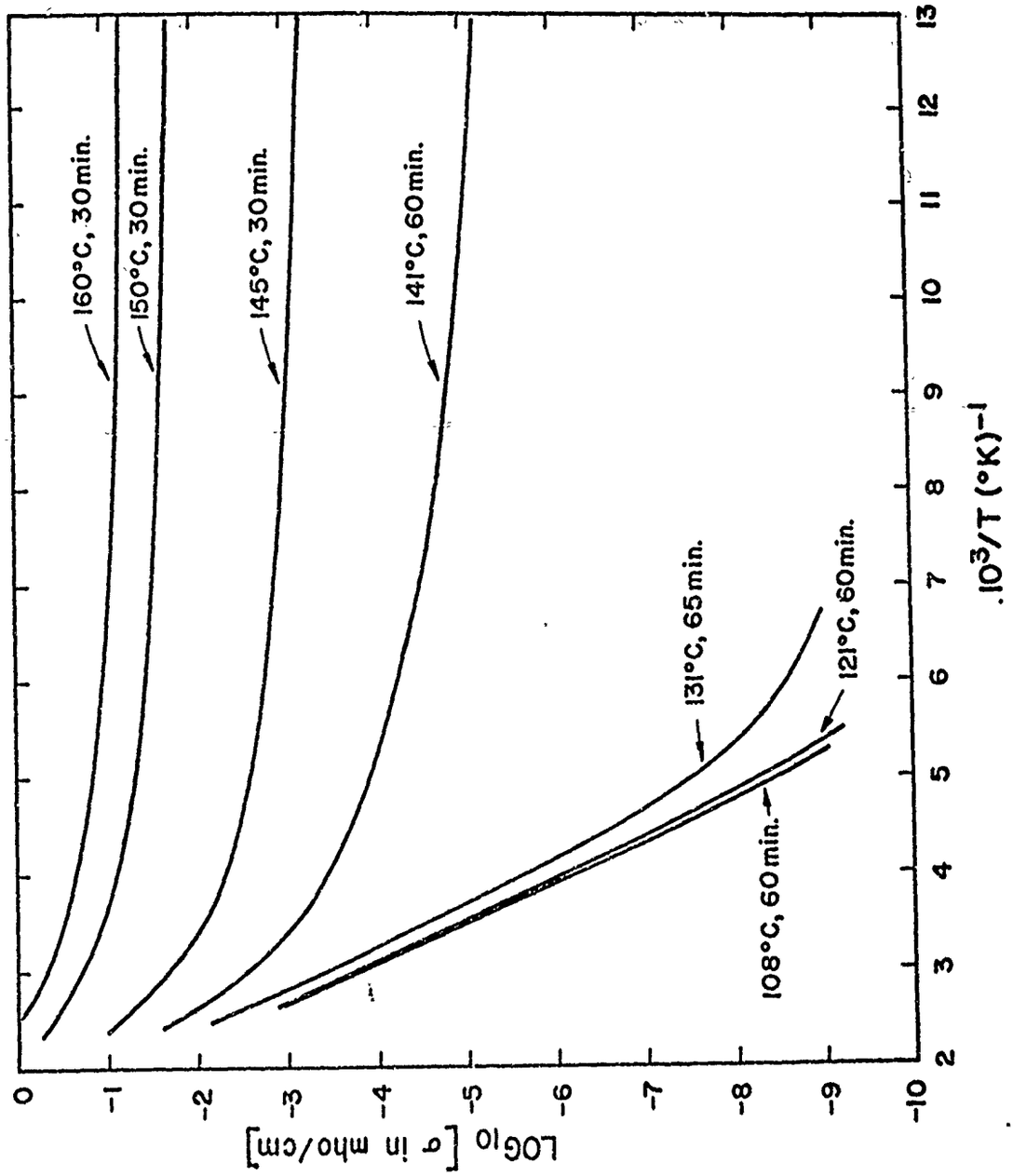
160°C, 30 min.
150°C, 30 min.
145°C, 30 min.
141°C, 60 min.
131°C, 65 min.
121°C, 60 min.
108°C, 60 min.
LOG10 [σ in mho/cm]
0
-1
-2
-3
-4
-5
-6
-7
-8
-9
-10
2
3
4
5
6
7
8
9
10
11
12
13
10³/T (°K)⁻¹

2.2.5 Thermally Stimulated Argon Effusion from Sputtered $GeTe_2$

The rf sputtering process occurs in an argon atmosphere at approximately 7 millitorr pressure. Sputtering onto unbiased substrates results in a significant level of argon entrapment. We have measured argon concentrations in sputtered chalcogenide films ranging up to several atomic percent, and have discovered that the temperature dependent rate of release of the trapped argon can give information concerning the accompanying phase transformations and the argon mobility in these various phases. An introduction to this technique and its application to sputtered amorphous $GeTe_2$ is given in the article by Fagen[4] (section 3.4.3 and Appendix I). We shall therefore limit our remarks here to a brief summary of this work and to the presentation of some recent results which extend it.

The sequence of phase changes which occur during the heating of amorphous $GeTe_2$ has been well characterized by scanning calorimetry and x-ray diffraction studies. Below the glass transition temperature, $T_g = 230^{\circ}C$, the amorphous phase is kinetically stable. Crystallization is not observed below this temperature, although annealing below T_g does produce significant changes in optical[3] and electrical[18] properties. A significant question is whether the release of trapped argon might account for these changes. Fagen tentatively concludes that this possibility is excluded because less than one percent of the trapped argon partial pressure is, however, observed below T_g, indicating a finite mobility of argon atoms through the interstices of this glass.

Above T_g the atomic mobility of the Ge and Te atoms is assumed to increase rapidly with temperature, by analogy to other liquid systems at corresponding temperatures. An increase in the slope of the argon partial pressure versus temperature is observed at this point, indicating an increased mobility for the trapped argon atoms as well. The increased atomic mobilities lead, in turn, to crystallization, which occurs for this alloy as the simultaneous spherulitic precipitation of Te and GeTe crystals over the approximate temperature range of 240 - 280°C (see section 2.2). The argon partial pressure curve has a maximum in the same temperature interval, suggesting a competition between the increasing mobility of argon in the liquid state and the decreasing volume fraction of liquid as crystallization proceeds.

Between the end of crystallization and the beginning of melting, the crystalline phases are thermodynamically and kinetically stable. In this temperature range the argon partial pressure increases nearly exponentially with temperature, indicative of another regime of thermally activated argon mobility, in this case occurring either within the crystalline GeTe and Te phases or along the boundaries between them. Below T_m and at this heating rate, most of the argon is retained so that the effective supply of argon atoms is essentially unlimited.

At about 380°C, the $GeTe_2$ sample begins to melt by transforming into a mixture of $Ge_{17}Te_{83}$ eutectic liquid and residual GeTe crystals

in approximately equal volume fractions. This event is accompanied by an abrupt increase in argon partial pressure, reflecting the substantially higher argon mobility in the liquid phase. As heating continues, a progressively larger volume fraction of the liquid phase is formed, presumably increasing the supply of argon available to the high mobility liquid state diffusion and effusion processes. Counter-balancing this increased supply is the rapid rate of argon exhaustion produced by the rapid effusion. At about 480°C nearly all the GeTe has melted, and nearly all the argon originally trapped in the sample has been expelled, leading to a rpaid decline in argon partial pressure which reaches the background level by the end of the experiment.

These sequential stages in the temperature dependent argon release kinetics can be further clarified by subjecting a sample to sequential heating cycles which terminate at certain of the phase transition temperatures. In Figure 2.8 we have plotted the results of such an experiment, and compared them to the electrical conductivity of a comparable sample subjected to the same sequence of heating cycles. Here the conductivity change with annealing and the argon effusion below T_g can be compared directly, confirming the absence of any obvious correlation between them. The thermally activated nature of the argon effusion process within any single structural regime (i.e., either glass or liquid or crystalline) is again apparent, but another characteristic feature of the effusion kinetics now emerges: the effusion rate at a given temperature is significantly less upon

Figure 2.8 Comparison of conductivity (left hand scale) and argon effusion rate (right hand scale) versus temperature for sputtered amorphous $GeTe_2$. Data obtained in these separate thermal cycles: A, 50 - 205°C (i.e. to completion of defect annealing); B, 50-270°C (i.e. to completion of crystallization); C, 50 - 470°C (i.e. to completion of argon release). Heating rate $\sim$ 5 deg. min^{-1}.

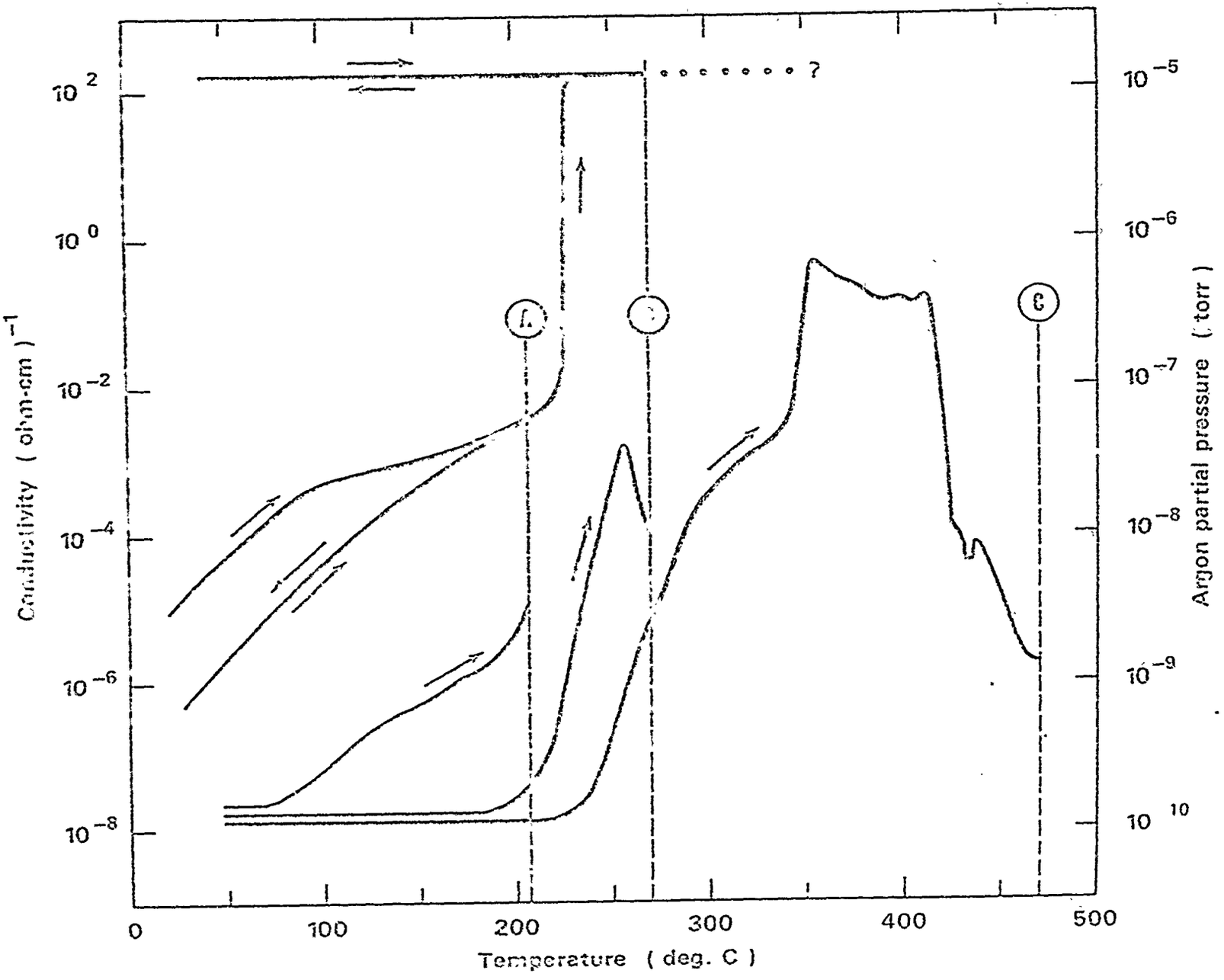
Conductivity (ohm-cm)$^{-1}$
10^{2}
10^{0}
10^{-2}
10^{-4}
10^{-6}
10^{-8}
Argon partial pressure (torr)
10^{-5}
10^{-6}
10^{-7}
10^{-8}
10^{-9}
10^{-10}
?
0
100
200
300
400
500
Temperature (deg. C)

reheating the sample to that temperature, indicating that the effusion rate at constant temperature decreases with the time spent at that temperature, even though the total argon content in the sample may be only slightly changed. These observation in turn indicate that we can consider the total argon content of the film to be present in the form of several species. Each species involves a different environment of argon atoms which has its own activation energy (or distribution of activation energies) for release of argon. Isothermal effusion studies would be required to sort out the detailed mechanism of argon migration and effusion within each structural regime.

2.2.6 Conclusions Regarding Atomic Structure of Amorphous Ge-Te Alloys

We have presented a variety of property measurements on sputtered amorphous Ge-Te alloys, and additional work on these alloys is currently in progress. These results permit the formulation of structural models which describe the chemical bonding in the amorphous Ge-Te system as a function of composition.

Apparently an ordered covalent network predominates for amorphous structures between Te and $GeTe_2$. The progressive increase in annealed electrical gap with the elimination of Te-Te bonds, and the increase of T_g with the addition of Ge cross-linking points give indirect support to such a model. The existence of T_g and E_g maxima and enthalpy and density minima at or near $GeTe_2$ are in full accord with a completely cross-linked ordered structure at this composition.

The addition of Ge to amorphous $GeTe_2$ does not produce the

smoothly varying properties which accompany the addition of Te to $GeTe_2$. Instead, the enthalpy data indicate a large negative departure from the ordered covalent network predicted mixture of 2-fold Te and 4-fold Ge, leading to a minimum at GeTe. This result can only be reconciled with a strong ordering tendency for the GeTe composition, which in turn can only be reconciled with the X-ray data by postulating the existence of a fully ordered 3-fold coordination of Te and Ge at GeTe. No conductivity singularity accompanies this structural singularity, perhaps because in this case the ordered phase has an electrical gap which lies near the gaps of the two pure end member amorphous phases, Ge and Te.

These models, while supported by other indirect observations such as relative ease of nucleation of crystalline Te and GeTe throughout the system, clearly demand direct experimental verification. It has been shown by Bienenstock, et al[9], that the neutron diffraction RDF for amorphous GeTe would distinguish between the 3-fold and the 2-fold plus 4-fold models. We feel that the time and expense required to sputter or evaporate a sufficiently large sample of amorphous GeTe for neutron diffraction would be well invested in terms of the scientific reward to be obtained, and hope to be able to collaborate on such an experiment in the near future. The proposed structure of $GeTe_2$, especially the presumed lack of Ge-Ge and Te-Te bonds in this alloy, will be the subject of additional X-ray RDF experimentation

in an effort to compare the observed X-ray diffraction with well verified tetrahedrally coordinated random network structures such as SiO_2 and GeO_2. In the meantime we find the proposed structures to be useful working models and are continuing our efforts to collect more indirect data in support of them. In addition we are investigating direct diffraction evidence of longer range correlation in these glasses and in the system $GeTe_2$ - $GeSe_2$. This work is still in a preliminary stage.

2.3 Sputtered Amorphous $GeTe_2$ - $GeSe_2$ Alloys: New Transport Measurements And Proposed Band Model

2.3.1 Introduction

As noted above, the prototypical amorphous chalcogenide $GeTe_2$ has received considerable attention at ECD by virtue of its stoichiometric and possible structural analogy to SiO_2, GeO_2 and other tetrahedrally coordinated random network glasses. In these glasses, a single chemical bond type, i.e., Ge-O, Si-O, etc., is found to account for the observed structural and physical properties. Abundant evidence has accumulated in the course of our studies to indicate that similar chemical ordering tendencies are significant for both $GeTe_2$ and $GeSe_2$, justifying our emphasis on the properties of these materials and mixtures of them. In this section we present some unpublished results on the photoconductivity of $GeTe_2$. In addition we have obtained extensive new data for the temperature dependence of thermopower and the effects of annealing on the thermopower for sputtered amorphous $GeTe_2$-$GeSe_2$ alloys. The new transport measurements, including some refined dc conductivity data for the same pseudo-binary alloys, have been combined with our previously reported optical absorption results[2,3] to construct a simplified band structure model which largely accounts for the optical and electrical properties of the virgin and annealed alloy films.

2.3.2 Photoconductivity of $GeTe_2$

2.3.2.1 Introduction

Band structure models for amorphous semiconductors characteristically

assume a high density of low mobility, spatially localized states in the tails of the valence and/or conduction bands. The existence of these states is inferred from photoconductivity[19], ac conductivity[20], high-field conductivity[21], and from a variety of other transport properties[22]. However, none of these measurements by itself is capable of defining the density of such states as a function of their energy or their position in space.

Nevertheless, a new analysis of photoconductivity results which places strong constraints on the allowable density of states has emerged from collaborative efforts between E. A. Fagen at ECD and R. Rube and T. Arnoldussen at Stanford University. This model (A.B.F.) is described in detail in a paper[23] by these authors which is included in appendix I of this report. The application of the A.B.F. model to the calculation of certain of states parameters for virgin and annealed sputtered amorphous $GeTe_2$ films is described below. We have emphasized the low temperature photoconductivity regime, i.e., the temperature range in which the photocurrent dominates the dark current. In this regime the temperature dependence of the photocurrent is controlled primarily by recombination traffic through one or both sets of localized states. Thus the density of these localized states can be inferred from the temperature dependence of photocurrent. For the $GeTe_2$ study we were primarily interested in the effect of annealing of the virgin films upon the calculated density of (valence band) trapping states.

2.3.2.2 Experimental Results and Model Calculations

The photocurrent and the dark current (with its current scale displaced downwards by 10^3) for virgin and annealed $GeTe_2$ are plotted for several light intensities as a function of reciprocal temperature in Figure 2.9. The experimental details are more fully described in that figure caption. All the photocurrent curves obtained display the familiar maximum near the temperature where the dark current and photocurrent are equal, with thermally activated regions at higher and lower temperatures. The values of certain band structure parameters have been calculated from these data by use of the A.B.F. model as shown in Figure 2.10. The decrease in low temperature photocurrent accompanying the annealing of $GeTe_2$ appears to result primarily from an increase in E_v^*, a parameter which characterizes the width of the valence band density of states tail. However, the relative increase in E_v^* (11%) is less than the relative increase in E_c (23%) $\approx 2\ E_f$, indicating that the width of the calculated valence band tail relative to the band gap decreases slightly with annealing if the results are normalized for the accompanying increase in band gap. These calculations provide an exceedingly helpful qualitative assessment of the role of annealing in affectinv the density of states function; however the quantitative results are sufficiently dependent upon assumptions inherent in the A.B.F. model to require confirmation by other techniques.

2.3.3 Thermoelectric Power of $GeTe_2$ - $GeSe_2$ Alloys

2.3.3.1 Introduction

Although an attempt to provide a detailed analysis

Figure 2.9 Temperature dependence of photocurrent and dark current in 0.5 μm sputtered thin film of $GeTe_2$ with coplanar molybdenum electrodes, before and after annealing at 205°C, for two different intensities of illumination. Intensity of $\approx 10^{15}$ photons/cm^2-sec at a wavelength of 1.0 μm.

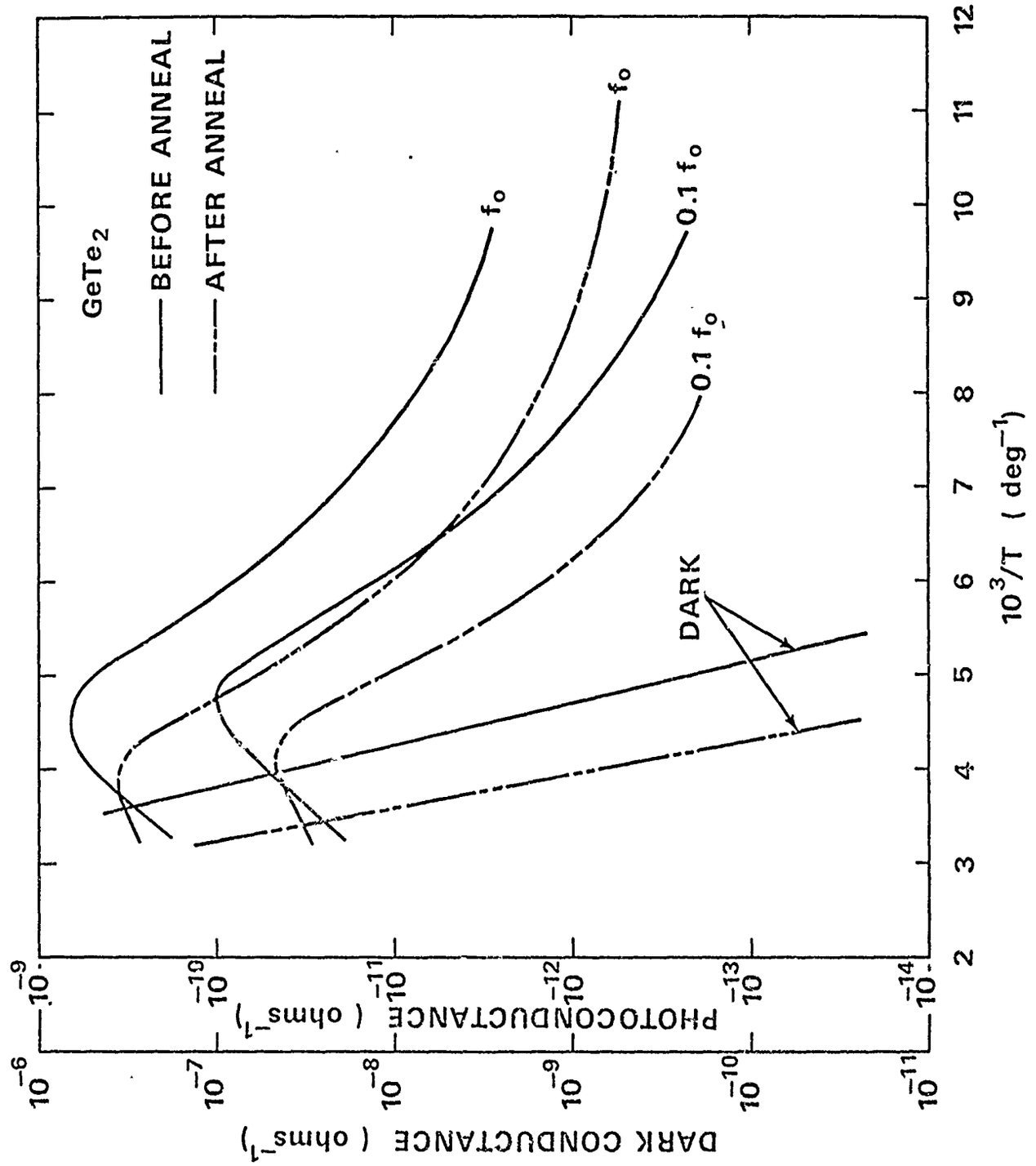
GeTe2
BEFORE ANNEAL
AFTER ANNEAL
fo
fo
0.1 fo
0.1 fo
DARK
DARK CONDUCTANCE (ohms-1)
PHOTOCONDUCTANCE (ohms-1)
10-3/T (deg-1)

Figure 2.10 Band structure parameters determined from the data of Fig. 2.9 by the methods of Ref. 23, under the assumption that transitions between sets of localized states at P_c^* and E_v^* dominate the recombination traffic. In order to assign numerical values to the various densities of states, the following disposable parameters have been chosen: the microscopic band mobility $\mu_o \approx 1$ cm^2/ V-sec, at all temperatures; the capture coefficient for a nuetral trap $C^o \approx 10^{-9}$ cm^3/sec; and the capture coefficient for a negatively charged trap $C^- \approx 10^{-5}$ cm^3/sec.

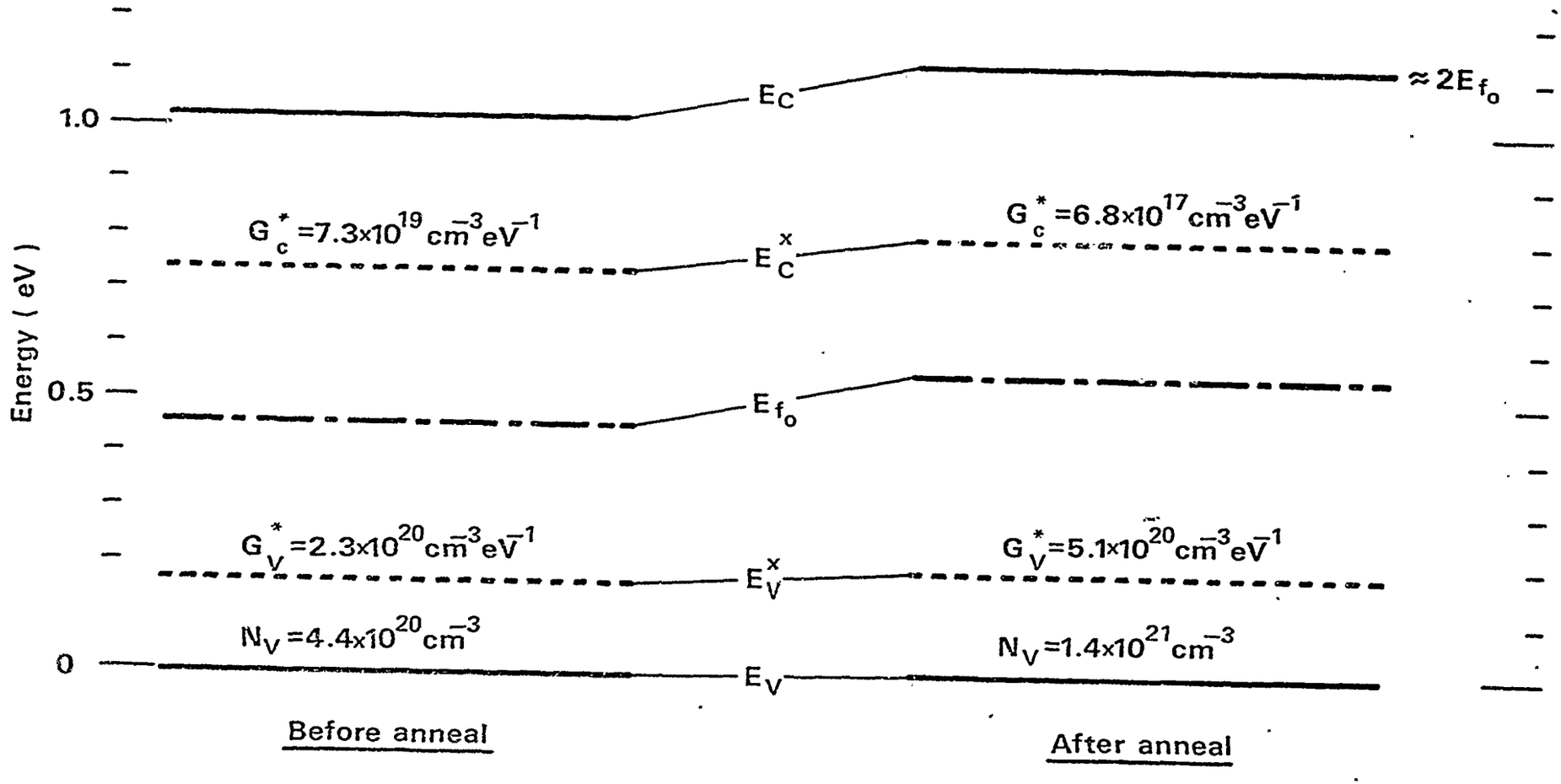
Energy (eV)
1.0
0.5
0
E_C
$\approx 2E_{f_o}$
$G_c^* = 7.3 \times 10^{19} cm^{-3} eV^{-1}$
E_C^x
$G_c^* = 6.8 \times 10^{17} cm^{-3} eV^{-1}$
E_{f_o}
$G_V^* = 2.3 \times 10^{20} cm^{-3} eV^{-1}$
E_V^x
$G_V^* = 5.1 \times 10^{20} cm^{-3} eV^{-1}$
$N_V = 4.4 \times 10^{20} cm^{-3}$
E_V
$N_V = 1.4 \times 10^{21} cm^{-3}$
Before anneal
After anneal

of the temperature and composition dependence of thermopower involves the entire spectrum of transport and band structure parameters, a two band semiconductor model serves to identify the majority carrier type and the relative roles of majority and minority carriers. The applicability of such a model has been confirmed by our earlier studies[2,18], by noting a close correspondence in some cases between the slope of the thermopower, S, versus reciprocal temperature and the electrical activation energy. Knowledge of the majority carrier type versus composition or structural state (in the case of annealing effects) can be combined with conductivity and optical absorption data within the context of the band conduction model to yield the approximate positions of the valence and conduction band edges and the Fermi level.

We selected the $GeTe_2$ - $GeSe_2$ sputtered amorphous film system for detailed thermopower measurements, because of our extensive experience with optical, electrical, and thermal studies of these films[2,3]. We wished also to study the effects of a changing band gap in a chalcogenide system whose atomic structure could be considered more or less fixed. For this pseudo-binary we consider that the short-range order consists of tetrahedrally coordinated Ge atoms, connected by Ge-Te-Ge and Ge-Se-Ge linkages in such a way that essentially all bonds are either Ge-Se or Ge-Te. Furthermore, the thermal data ($T_g(x)$) would be inconsistent with any significant clustering tendency among like bonds and X-ray diffraction revealed none of the features associated with phase separation, even after long anneals

just below T_g. Thus we visualize this system as a potentially ideal random solution of Ge-Te and Ge-Se bonds all sharing a common coordination structure. The accumulating evidence for such a simplified structural model permits the analysis of thermopower, a subtle transport behavior probe, without introducing arbitrary structural hypotheses (e.g., phase separation, partial crystallization, etc.) to account for the observed results. In addition, both the positional and compositional disorder favor a CFO model in the density of states.

An additional complexity arises in conjunction with the analysis of electronic transport in sputtered amorphous semiconducting films, involving the role of defects in controlling the band structure of the films prior to any annealing. We have observed and reported the effects of annealing upon the dc conductivity, optical absorption and thermopower of several $GeTe_2$-$GeSe_2$ alloys[2,3,18], and have observed these effects in most other sputtered amorphous samples (except those whose T_g is below about 130°C and which presumably anneal during deposition). These changes in band structure with annealing appear to occur at temperatures where atomic mobility is negligible, and, indeed, we can find little X-ray evidence in the chalcogenides for significant atomic rearrangements accompanying them. Extensive studies of analogous effects in evaporated and sputtered amorphous Si and Ge thin films[25] have been interpreted in the past in terms of the removal and coalescence of voids whose interior surfaces contribute localized defect states,

smearing out the top of the valence band. As these voids are removed, or as their surface area is reduced via coalescence, the concentration of these defect states is reduced and their dominance over bulk electronic properties, at least at high temperatures, is lost. To our knowledge, the density of states function for a defective amorphous Ge or Si sample has not been experimentally determined, so the nature of the assumed band smearing and introduction of the defect-associated localized states is still speculative. More recently our own work (see section 3 and Appendix II) has clearly demonstrated a structural distinction between sputtering and other forms of deposition. The difference due to impurities makes a singificant contribution to the density of states and attendent optical properties.

For Si and Ge, no T_g has ever been observed either thermally or mechanically (i.e., via a direct measurement of viscosity), and our own observations of the thermal annealing of defects in sputtered Ge indicate that crystallization begins before defect annealing has terminated. One ultimate goal of our materials survey work is to correlate band structure and electronic properties with atomic structure. Clearly, then, the annealed amorphous solid with well known atomic structure is the ideal point of departure. The $GeTe_2$ - $GeSe_2$ sputtered alloys meet this requirement because they all have demonstrable T_g's, indicating that any structural defects introduced during sputtering can, in principle, be removed by annealing at or above T_g before any crystallization can occur. The changes in electronic properties (optical absorption and

transport) which accompany defect removal can be considered as a bonus, providing an indirect description of the band structure of the defective glass.

2.3.3.2 Experimental Results

The temperature dependence of the thermopower of various alloys in the $GeTe_2$ - $GeSe_2$ system is shown in Figure 2.11 in which we have plotted the Seebeck Coefficient, S, versus reciprocal absolute temperature for the virgin and for the fully annealed films. A plot of the conductivity and conductivity activation energy ΔE_o, at 96^oC is shown in Figure 2.12. The virgin films all obey the relation $S = BT^{-1}-C$, and the values of B correspond approximately to the relationship $eB = \Delta E_o$, where ΔE_o is the conductivity activation energy. Since S and B are positive for the virgin (defective) films, and since $eB \approx \Delta E_o$, the intrinsic semiconductor model indicates that the motion of holes in the valence band is the dominant conduction mechanism for all of the virgin films.

A progressive increase of the effect of annealing upon S is observed with increasing $GeSe_2$ concentration, as indicated in Figure 2.11. Alloys containing 50% or more of the $GeSe_2$ component (including our preliminary results on the 90% and 100% $GeSe_2$ alloys) have negative Seebeck coefficients for all experimentally accessible temperatures. Only for the $GeTe_2$ alloy does the one band semiconductor model appear applicable to annealed alloys. For this alloy $eB \approx +\Delta E_o$, indicating hole conduction in the valence band. For intermediate alloys, a

Figure 2.11 Thermopower (Seebeck coefficient S) versus $10^3/T$ for amorphous $(GeTe_2)_{1-x}(GeSe_2)_x$ virgin and annealed sputtered alloy films.

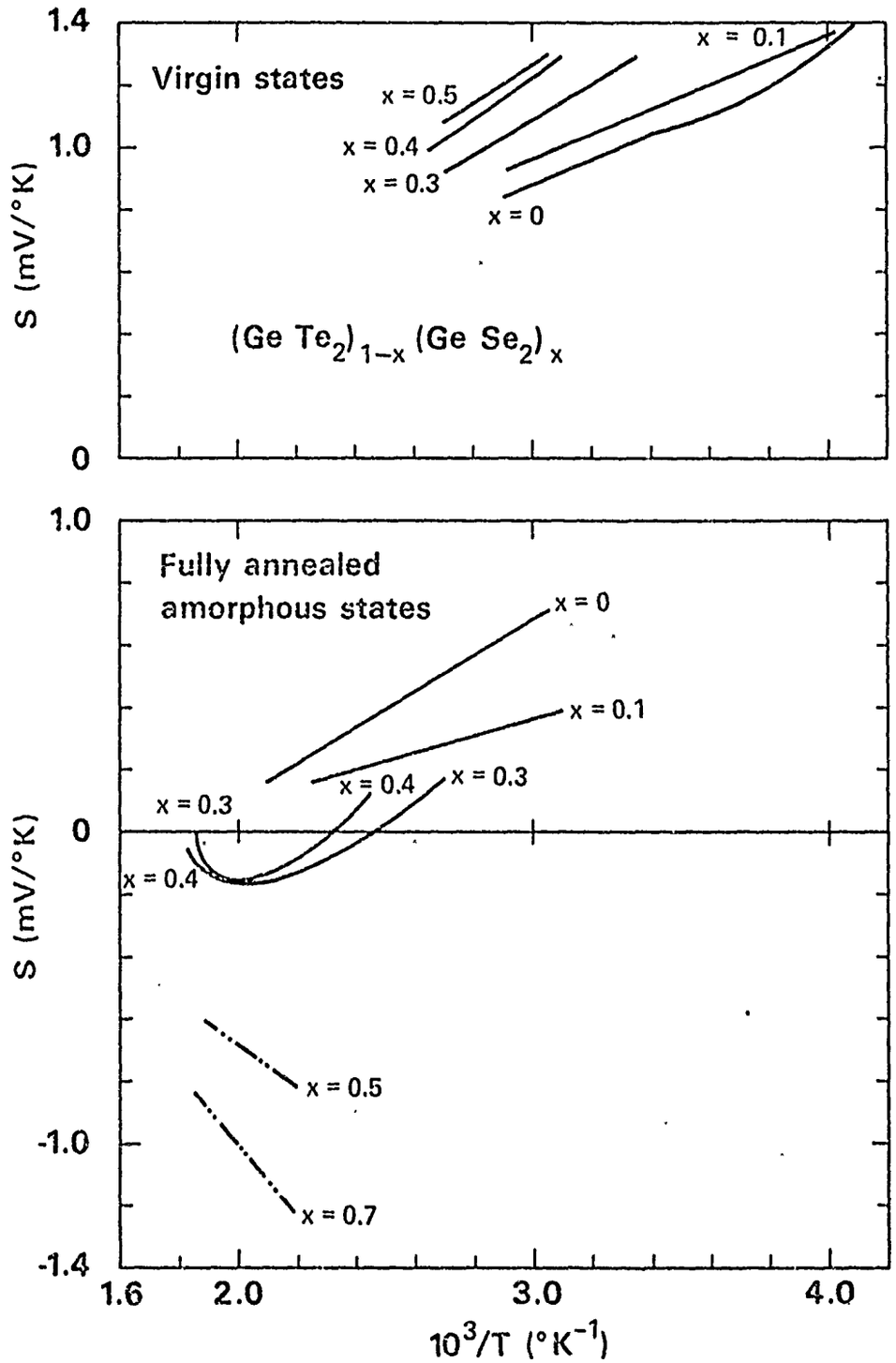
Virgin states
x = 0.5
x = 0.4
x = 0.3
x = 0.1
x = 0
(Ge Te2)1−x (Ge Se2)x
S (mV/°K)
1.4
1.0
0
Fully annealed
amorphous states
x = 0
x = 0.1
x = 0.4
x = 0.3
x = 0.3
x = 0.4
x = 0.5
x = 0.7
1.0
0
-1.0
-1.4
1.6
2.0
3.0
4.0
10³/T (°K⁻¹)

Figure 2.12 Electrical conductivity and conductivity activation energy at 96°C versus composition for amorphous $(GeTe_2)_{1-x}$ $(GeSe_2)_x$ virgin and annealed sputtered films. Tangents of $\ln\sigma$ versus $10^3/kT$ at 96°C were used for activation energies.

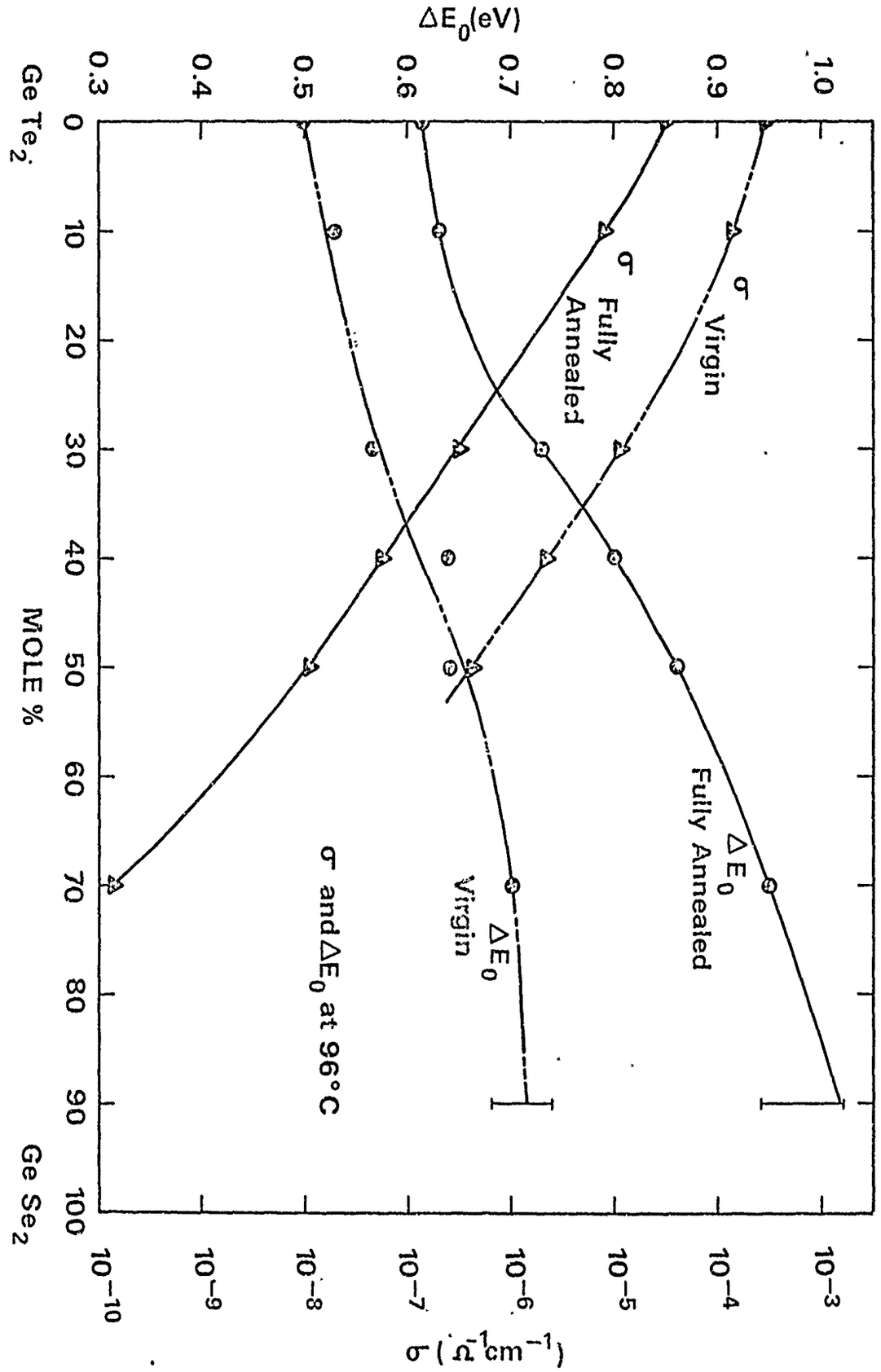
ΔE0(eV)
0.3
0.4
0.5
0.6
0.7
0.8
0.9
1.0
Ge Te2
0
10
20
30
40
50
60
70
80
90
100
Ge Se2
MOLE %
σ Fully Annealed
σ Virgin
ΔE0 Fully Annealed
ΔE0 Virgin
σ and ΔE0 at 96°C
10−10
10−9
10−8
10−7
10−6
10−5
10−4
10−3
σ (Ω−1cm−1)

mixture of electron and hole conduction appears to affect the value of S in accordance with the two band semiconductor model predictions:

$$S = \frac{\sigma_h - \sigma_e}{\sigma_h + \sigma_e} \frac{k}{e} \left(\frac{\Delta E_o}{kT} - \frac{\beta}{2k} + A \right) \qquad (1)$$

Considering the compositional dependence of ΔE_o and β for the annealed alloys, as S and β decrease, ΔE_o increases, indicating a progressive increase in σ_e relative to σ_h as Se is substituted for Te.

The detailed effects of annealing upon thermopower and conductivity emerge from an examination of S and σ, $edS/d(1/T)$ and ΔE_o, at 96°C versus annealing temperature, as plotted in Figures 2.13 and 2.14, respectively. If data at 96°C were unavailable due to experimental limitations, the original data were extrapolated to give points at 96°C. Such extrapolated information is indicated by broken lines in the figures. Note that the entire change in the conductivity (aside from crystallization) takes place below T_g and does not change in the vicinity of T_g. The values of S and $edS/d(1/T)$ continue to show annealing effects above T_g, indicative of subtle changes in transport mechanism which are not reflected in the conductivity itself. We speculate that these changes in S at or above T_g are associated with minor changes in short range order. These arise because the sputtering process produces the glassy phase under conditions where atomic mobility may be extremely limited, leading to a higher energy bonding configuration (less short range order) in the sputtered glass than would

Figure 2.13 Thermopower and electrical conductivity at 96°C versus annealing temperature for sputtered $(GeTe_2)_{1-x}$ $(GeSe_2)_x$ alloys. Small arrows in the lower figure indicate glass transition temperatures. The large arrow for $GeTe_2$ represents crystallization.

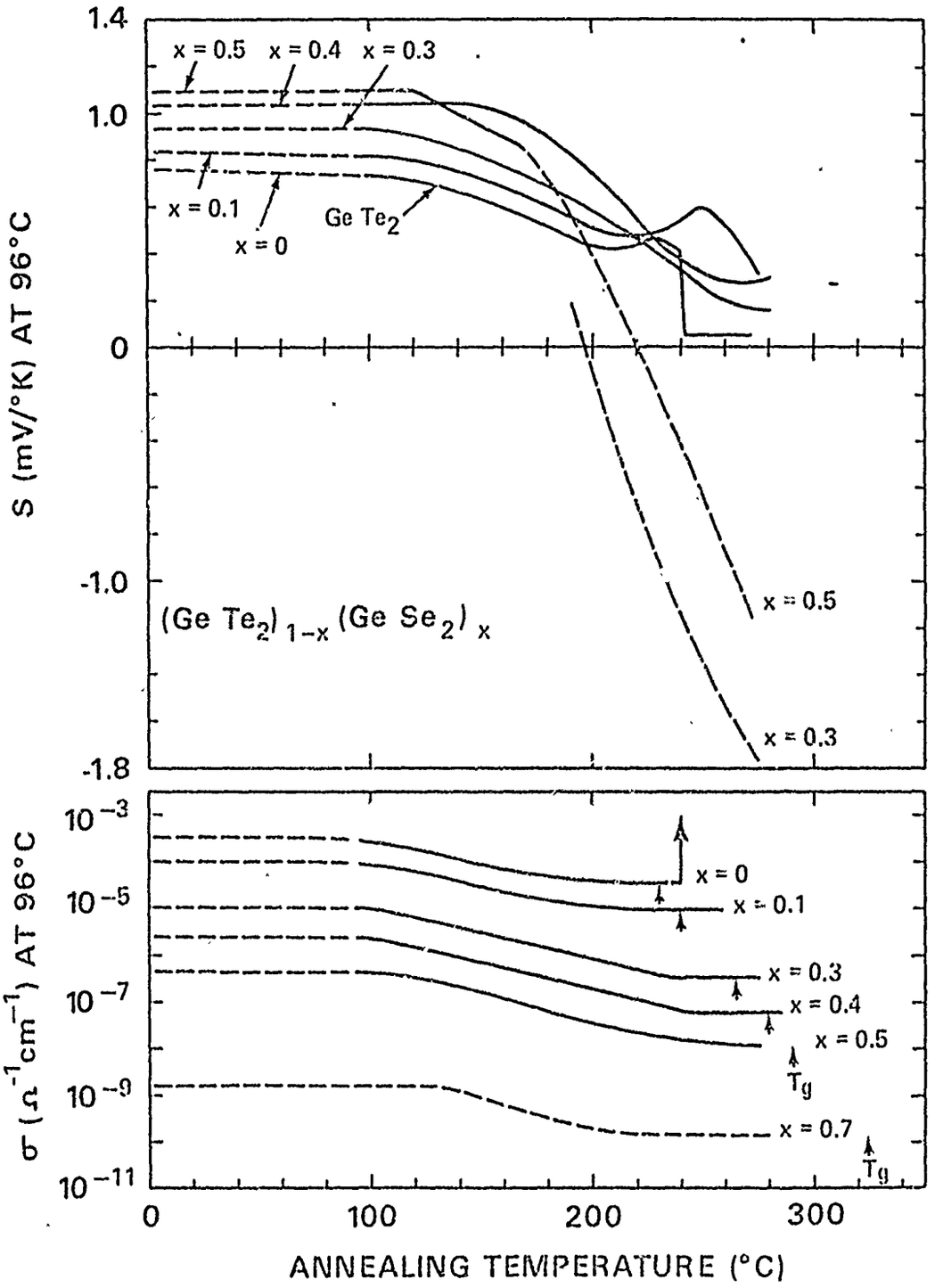
1.4
1.0
0
-1.0
-1.8
x = 0.5
x = 0.4
x = 0.3
x = 0.1
x = 0
Ge Te2
(Ge Te2) 1-x (Ge Se2) x
x = 0.5
x = 0.3
S (mV/°K) AT 96°C
10-3
10-5
10-7
10-9
10-11
x = 0
x = 0.1
x = 0.3
x = 0.4
x = 0.5
Tg
x = 0.7
Tg
σ (Ω-1cm-1) AT 96°C
0
100
200
300
ANNEALING TEMPERATURE (°C)

Figure 2.14 Electrical conductivity and Seebeck coefficient activation energies at 96°C versus annealing temperature for sputtered $(GeTe_2)_{1-x}(GeSe_2)_x$ alloys.

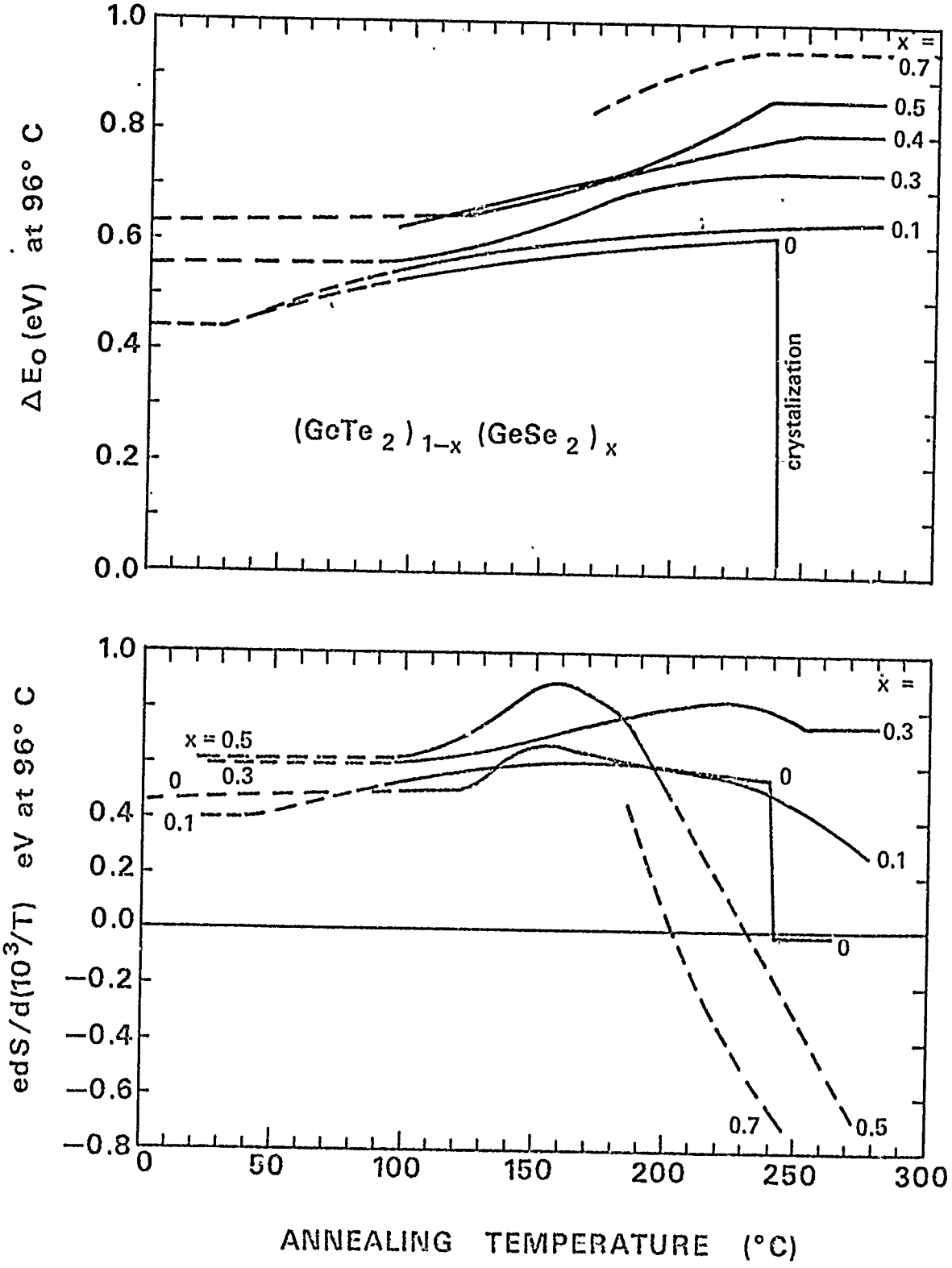
1.0
0.8
0.6
0.4
0.2
0.0
ΔEo (eV) at 96° C
x =
0.7
0.5
0.4
0.3
0.1
0
crystalization
(GeTe 2) 1–x (GeSe 2) x
1.0
0.4
0.2
0.0
−0.2
−0.4
−0.6
−0.8
edS/d(10³/T) eV at 96° C
x = 0.5
0
0.3
0.1
x =
0.3
0
0.1
0
0.7
0.5
0
50
100
150
200
250
300
ANNEALING TEMPERATURE (°C)

prevail in the supercooled metastable liquid state at T_g. However this ordering tendency appears to be an inadequate explanation for the annealing effects which occur for both S and σ well below T_g, due to the very low predicted atomic mobilities at these temperatures.

2.3.4 A Band Level Picutre of $GeTe_2$ - $GeSe_2$ Films: The Effect of Annealing

In this section we combine our new transport measurements with our earlier optical absorption data[2,3] to present a unified picture of the band structure of $GeTe_2$-$GeSe_2$ alloys as functions of composition and state of annealing. As might be anticipated, the gross features of the band structure, i.e., the positions of the band edges and the Fermi level, are more easily determined than the subtle features such as the density of states within the gap. Of the measurements here reported, only photoconductivity yields information concerning these states, information which must be derived indirectly (according to our present models) by a consideration of the transport of photoexcited carriers in band states. Until a more satisfactory method of directly measuring the density of states is available, the indirect approach via photoconductivity remains the most suitable approach.

In the model building described below, however, we shall ignore the localized states. These partially filled low mobility states manifest themselves indirectly in this model through their role in establishing the Fermi level, whose position will in effect be treated as a disposable parameter. The model we have chosen, then, corresponds in general to an asymmetrical two

band semiconductor, and the only parameters to be determined are the band gap and the Fermi level as functions of composition and state of anneal.

The ratio of the measured electrical activation energy, ΔE_o, to the "optical absorption gap", ΔE_{opt} (arbitrarily defined as the energy at which the absorption coefficient, α, equals 10^4 cm^{-1})[2] is plotted versus composition in Figure 2.15 for both virgin and annealed materials. For annelaed $(GeTe_2)_{1-x}(GeSe_2)_x$ films, this ratio peaks near $x = 0.5$, while the thermoelectric data indicate p-type conduction for $x \lesssim 0.4$ and n-type conduction for $x \gtrsim 0.5$. We therefore propose that in annealed compositions from $x = 0$ to $x = 1$, the Fermi level starts below the gap center, passes through the gap center at $x \approx 0.5$ and stays above the gap center for $x \gtrsim 0.5$. By normalizing the $\Delta E_o/\hbar\omega\,(10^4\ \text{cm}^{-1})$ data to the gap center at $x = 0.5$ for the annealed state, the relative position of the Fermi level in the gap can be plotted for the alloy system. That is, at $x = 0.5$,

$\frac{E_f - E_v}{E_c - E_v} = \frac{E_c - E_f}{E_c - E_v} = 0.5$. Assuming that $\frac{\Delta E_o}{\hbar\omega(10^4 \text{cm}^{-1})} = G\frac{E_f - E_v}{E_c - E_v}$ for $x \leq 0.5$, and $G\frac{E_c - E_f}{E_c - E_v}$ for $x \geq 0.5$, with G independent of composition and determined at $x = 0.5$ for the annealed state, the band edges and Fermi level are shown in Figure 2.16 for the annealed state. Using the same value of G for virgin materials, the energy levels for virgin alloys are given in Figure 2.17. Since it is also assumed that $E_c - E_v = \hbar\omega(10^4 \text{cm}^{-1})$ in these figures, the vertical scale is only approximate.

The choice of another convention for $E_c - E_v$ based on optical absorption would not greatly alter Figures 2.16 and 2.17 although the vertical scales would

Figure 2.15 Ratio of conductivity activation energy to "optical gap" for virgin and annealed sputtered $(GeTe_2)_{1-x}$ $(GeSe_2)_x$ alloys. Tangents of $\ln\sigma$ versus $10^3/kT$ at 96^oC are used for activation energies and the photon energies for which the optical absorption coefficient equals $10^4 cm^{-1}$ are used as "optical gaps".

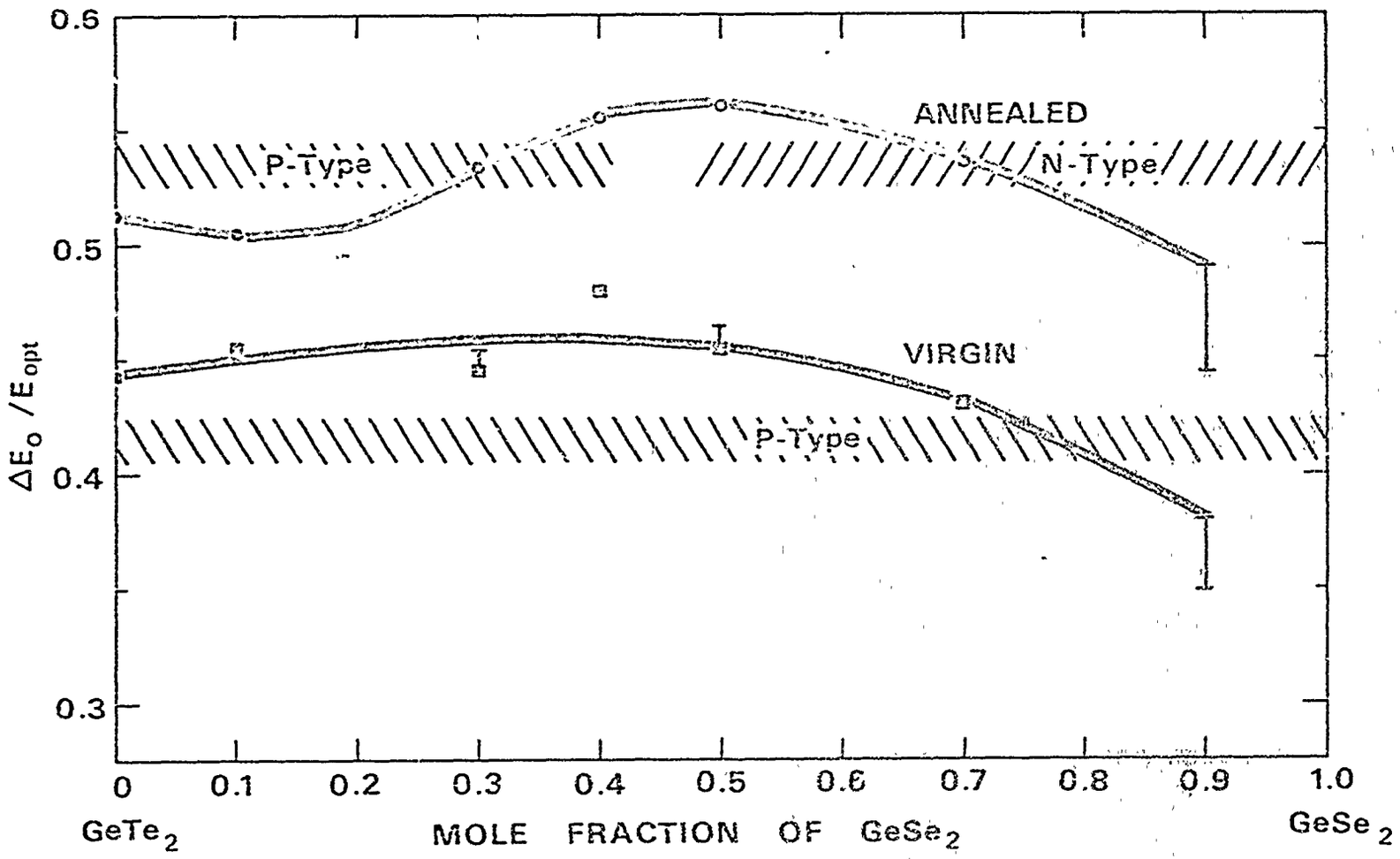
0.6
0.5
0.4
0.3
ANNEALED
P-Type
N-Type
VIRGIN
P-Type
$\Delta E_o / E_{opt}$
0
0.1
0.2
0.3
0.4
0.5
0.6
0.7
0.8
0.9
1.0
$GeTe_2$
MOLE FRACTION OF $GeSe_2$
$GeSe_2$

56-A

Figure 2.16 Energy level diagram versus composition for amorphous annealed $(GeTe_2)_{1-x}$ $(GeSe_2)_x$ alloys showing relative positions of valence and conduction band (or mobility) edges and the Fermi level. Vertical scale is approximate.

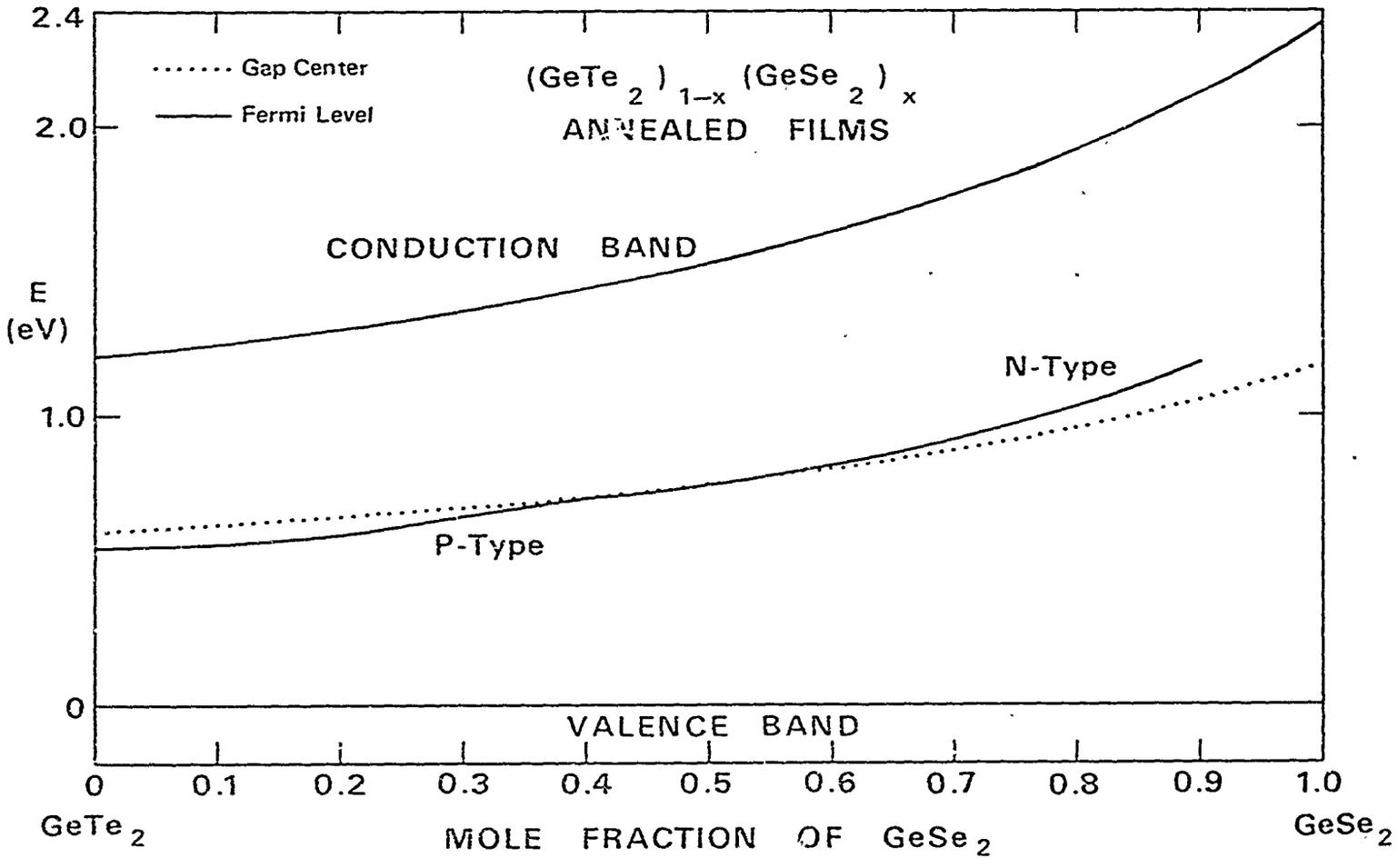
2.4
2.0
1.0
0
E
(eV)
Gap Center
Fermi Level
$(GeTe_2)_{1-x}(GeSe_2)_x$
ANNEALED FILMS
CONDUCTION BAND
N-Type
P-Type
VALENCE BAND
0
0.1
0.2
0.3
0.4
0.5
0.6
0.7
0.8
0.9
1.0
$GeTe_2$
MOLE FRACTION OF $GeSe_2$
$GeSe_2$

57-4

Figure 2.17 Energy level diagram versus composition for amorphous virgin $(GeTe_2)_{1-x}$ $(GeSe_2)_x$ sputtered alloys showing relative positions of valence and conduction band (or mobility) edges and the Fermi level. Vertical scale is approximate.

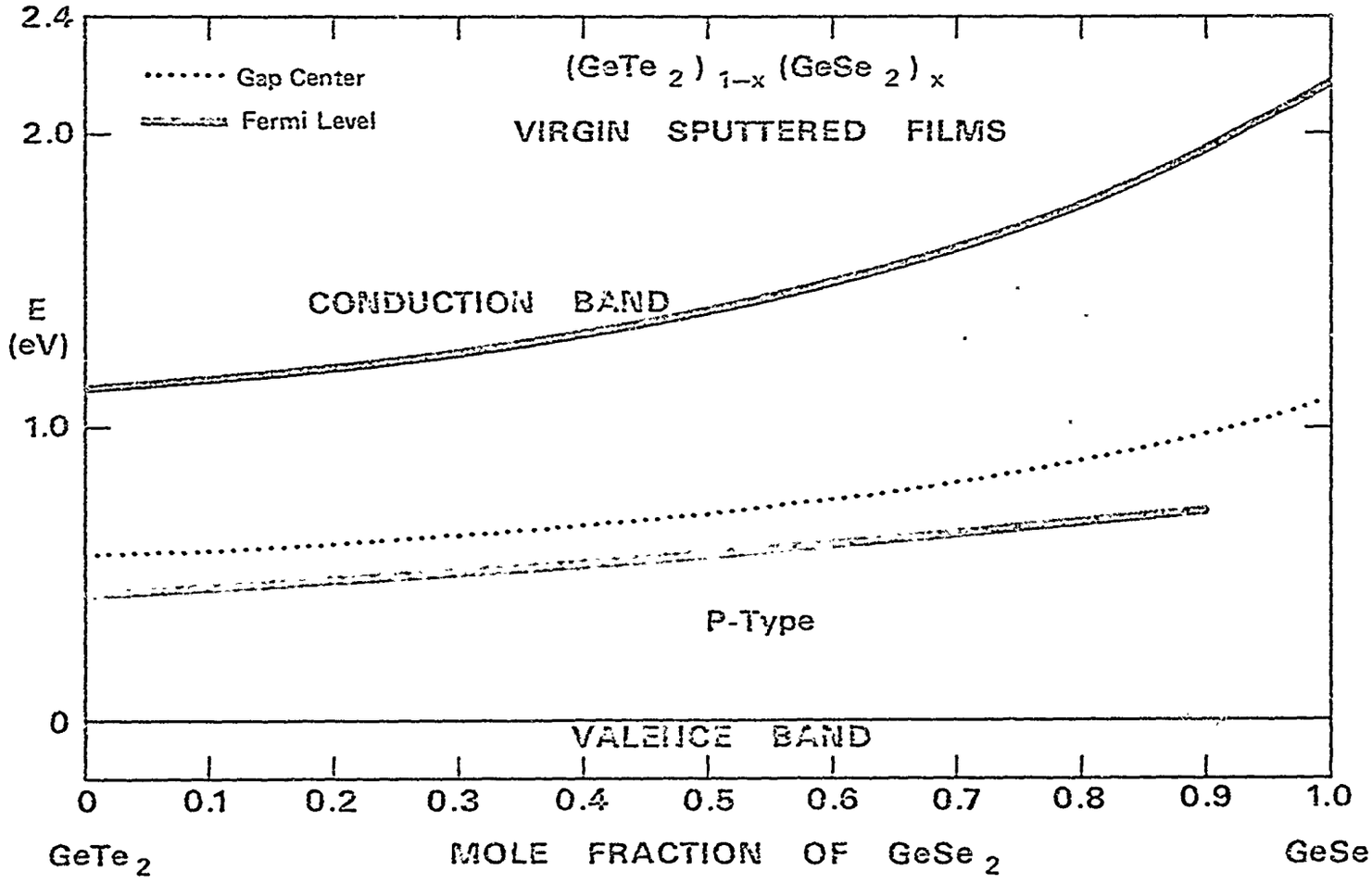
2.4
2.0
1.0
0
E
(eV)
Gap Center
Fermi Level
$(GeTe_2)_{1-x}(GeSe_2)_x$
VIRGIN SPUTTERED FILMS
CONDUCTION BAND
P-Type
VALENCE BAND
0
0.1
0.2
0.3
0.4
0.5
0.6
0.7
0.8
0.9
1.0
$GeTe_2$
MOLE FRACTION OF $GeSe_2$
$GeSe_2$

be changed. Also, G as defined above probably is not completely independent of composition and annealing, but it is unlikely, in this simple pseudo-binary with one Group VI element being replaced by another, that G varies drastically.

The following qualitative features of Figures 2.16 and 2.17 are independent of the quantitative assumptions:

1) In virgin materials E_f is on the valence band side of the gap for all compositions.

2) E_f is further from the gap center for virgin materials than for annealed materials.

3) Annealing moves the Fermi level away from the valence band at all compositions.

4) Annealed $GeTe_2$ is p-type, whereas annealed $GeSe_2$ is n-type (based on an extrapolation from $x = 0.9$).

5) The ratio $E_f/(E_c - E_v)$ of the annealed alloys moves continuously from <0.5 to > 0.5 from $GeTe_2$ to $GeSe_2$.

6) In virgin materials, alloying brings E_f away from the valence band, as evidenced by $E_f/(E_c - E_v)$.

7) As previously known, annealing increases the band gap.

Speculations on the explanations of the above features:

1) Virgin Materials are p-type because the valence band edge is sharper than that of the conduction band edge. Mixing $GeTe_2$ and $GeSe_2$ reduces the sharpness of the valence band edge, resulting in the small rise in $\Delta E_o/\hbar\omega$ ($10^4 cm^{-1}$) for mixed virgin materials in Fig. 2.15.

2) Annealing sharpens the conduction band edge more than it affects the already sharp valence edge.

3) Annealed $GeSe_2$ and $GeTe_2$ have opposite conductivity types in spite of the assumed structural similarity. This is not understood, though it is provocative to note that the trend is in the same direction as found[26] for a number of III-V and II-VI crystalline semiconductors; i.e., the tendency toward n-type (p-type) behavior due to native defects increases as the atomic number of the cation decreases (increases).

The effectiveness of such a simplified model in accounting for the observed optical and transport properties is pleasing. The effect of annealing upon the Fermi level begins to provide an indication of the density and depth of the electronic states associated with the defects. In future studies we hope to use ac conductivity to help map the relative densities of the localized states near the Fermi level as a function of annealing history.

2.4 Survey Studies of High T_g Ternary and Pseudo-Ternary Chalcogenide Systems

2.4.1 Introduction

Our survey of chalcogenide glasses has emphasized the relationship between chemical composition, atomic structure, and the glass transition phenomenon. Inasmuch as crystallization and softening are the most probable causes of failure for any amorphous alloy device, whether optical, electrical or structural, we have focused considerable effort on the determinants of T_g, which often determines the threshold

for crystallization and flow phenomena. Our initial approach to this problem was to assume that the chalcogen saturated compositions, (i.e., those whose stoichiometry allows for complete cross-linking of the chalcogen chains or rings to form a random network of the GeS_2 or As_2S_3 sort) or mixtures of them, would lead to the highest T_g's. The results presented in the first two Semi-Annual Technical Reports of this contract[1,2] indicated that maxima in T_g are uncommon in pseudo-binary mixtures of chalcogen saturated compositions (we found none), so that no increase in T_g by the addition of new components to a binary composition can be expected if chalcogen saturation is maintained. The highest measured T_g among binary chalcogen saturated compositons is the 430°C of GeS_2, a value which has recently been confirmed[27]. While this is indeed a high T_g, we wondered whether it were possible to achieve comparable values of T_g in lower band gap materials. GeS_2 has an optical gap of approximately 3 eV, and many of the interesting chalcogenide switching and memory effects occur more commonly in materials with optical gaps of less than 1.5 eV.

An encouraging approach to this problem was reported in the Second Semi-Annual Technical Report[2], and consisted of the discovery of a region of T_g maxima in the Si-As-Te system along the line connecting As to SiTe. The highest T_g which we measured along this line was 438°C for $Si_{40}As_{20}Te_{40}$, which appears to be at or near the maximum for the entire ternary system. These glasses have band gaps of the order of 1.5 - 1.6 eV, but have the disadvantage of

containing Si, which imparts its oxide optical absorption bands to all but the most carefully prepared samples, and tends to accentuate the oxidation and crystallization of thin films via its reaction with moisture. In addition, our switching studies of thin film samples in this ternary system indicated extraordinarily high breakdown fields, which limit potential switching applications to very thin films. We therefore tried to apply the concept of average coordination number, which appeared to control the values of T_g observed in this ternary system, to other chalcogenide systems. Two of our goals were, (a) to obtain lower gap glasses without unduly lowering T_g, and (b) to reduce or eliminate the Si to optimize these glasses for optical and electronic device applications.

The maxima in T_g along the SiTe-As join originally suggested to us the importance of 3-fold average coordination in producing the strongest random network[3]. We continued to assume local satisfaction of valency (i.e., covalent binding for each atom) with the coordination number being given by the 8 - n rule. However, our recent thermodynamic measurements in the Ge-Te system strongly suggest an alternative binding scheme in the vicinity of the GeTe composition, involving a significant ionic component (i.e., partial transfer of one electron from a Te atom to a Ge atom) and resulting in an ordered three-fold coordinated structure (see section 2.2). While we have not examined the structural or thermodynamic evidence for such bonding effects in the ternary glasses along the SiTe-As

join, we now consider the partially ionic model and the resulting three-fold coordination the most sensible hypothesis to account for the high T_g's in these glasses.

2.4.2 Experimental Results

We have performed extensive T_g measurements in the SiTe-GeTe-As pseudo-ternary system in order to extend the application of the three-fold coordination model toward lower band gaps and lower T_g's, and to evaluate the trade-off between these two parameters. The T_g data are plotted in Figure 2.18, revealing a large area of glass formation in this system. The compositions which yielded a homogeneous glass in whole or in part are represented by dots on the ternary triangle. Except for the low T_g arsenic-rich corner which was not thoroughly studied, the area embraced by these samples constitutes the region of glass formation for 5 - 10 g samples melted at 1100°C in quartz glass ampoules and quenched into a water bath. All calorimeter samples were examined by reflection optical microscopy to confirm the absence of crystals. The T_g isotherms indicate a continuous decline in T_g as GeTe is substituted for SiTe, for all ratios of (SiTe + GeTe): As. This decline is steep at first, and then becomes much more gradual. The positions of the isotherms in the middle of the system are somewhat uncertain due to the approximately $\pm$ 10°C spread in the measured values and the nearly flat nature of the T_g surface in this area.

The observed T_g values are very high, in the sense that no

Figure 2.18 Glass transition temperature isotherms in the pseudo-ternary system 1/2 SiTe - 1/2 GeTe-As. Solid points indicate compositions which could be obtained as single phase homogeneous glasses, based on reflection optical microscopy.

64-A

previously reported T_g in the Ge-Te-As system exceeded 260°C[28]. We suspect that this plane represents a surface of maximum T_g's in the quaternary Si-Ge-As-Te system, i.e., that increases or decreases in the (Si + Ge): Te ratio would result in reductions in T_g. We are currently preparing samples to test this hypothesis.

The addition of GeTe to glasses on the SiTe-As join shows the results obtained to date on three bulk samples, all containing 30 atomic percent As, but differing in their SiTe;GeTe ratios. Again we see a sharp decrease followed by a leveling off of the activation energy, and an analogous increase and leveling off of the conductivity. These trends correlate well with the T_g trends, suggesting a casual relationship among them. Preliminary conductivity data for well annealed sputtered films agree with the bulk glass data, although the activation energy before annealing in the vicinity of 200°C is about 0.15 eV lower.

The three-fold coordination model for predicting maximum T_g in a multicomponent chalcogenide system has been applied to the pseudo-binary GeAsSe-GeAsTe system, and the results are plotted in Figure 2.20. We observe a well behaved $T_g(x)$ function which flattens out in the vicinity of GeAsTe at a value of about 340°C, the same T_g range which occurred in much of the GeTe-SiTe-As pseudo-ternary system. Published information on the Ge-As-Te system[28,29] does not indicate the possibility of glass formation at the GeAsTe

Figure 2.19 Activation energy and electrical conductivity at 25°C of three bulk glasses in the 1/2 GeTe - 1/2 SiTe - As pseudo-ternary system versus (Si: Si + Ge) ratio.

66-A

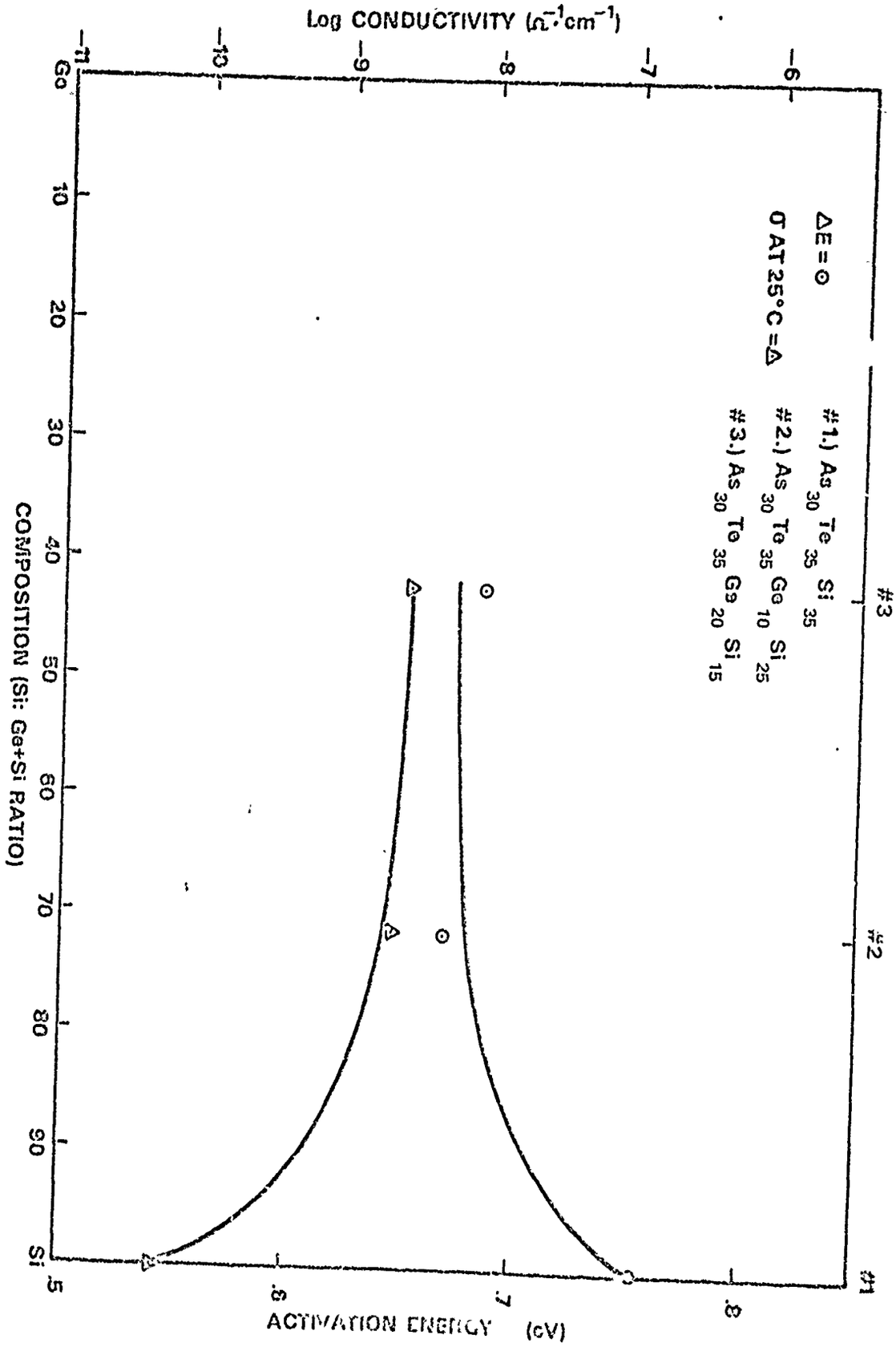
Log CONDUCTIVITY ($\Omega^{-1}cm^{-1}$)
-11
-10
-9
-8
-7
-6
Ge
10
20
30
40
50
60
70
80
90
Si
COMPOSITION (Si: Ge+Si RATIO)
.5
.6
.7
.8
ACTIVATION ENERGY (eV)
#1
#2
#3
ΔE = ⊙
σ AT 25°C = Δ
#1.) $As_{30}Te_{35}Si_{35}$
#2.) $As_{30}Te_{35}Ge_{10}Si_{25}$
#3.) $As_{30}Te_{35}Ge_{20}Si_{15}$

Figure 2.20 Glass transition temperature versus composition for bulk glasses in the GeAsTe - GeAsSe pseudo-binary system.

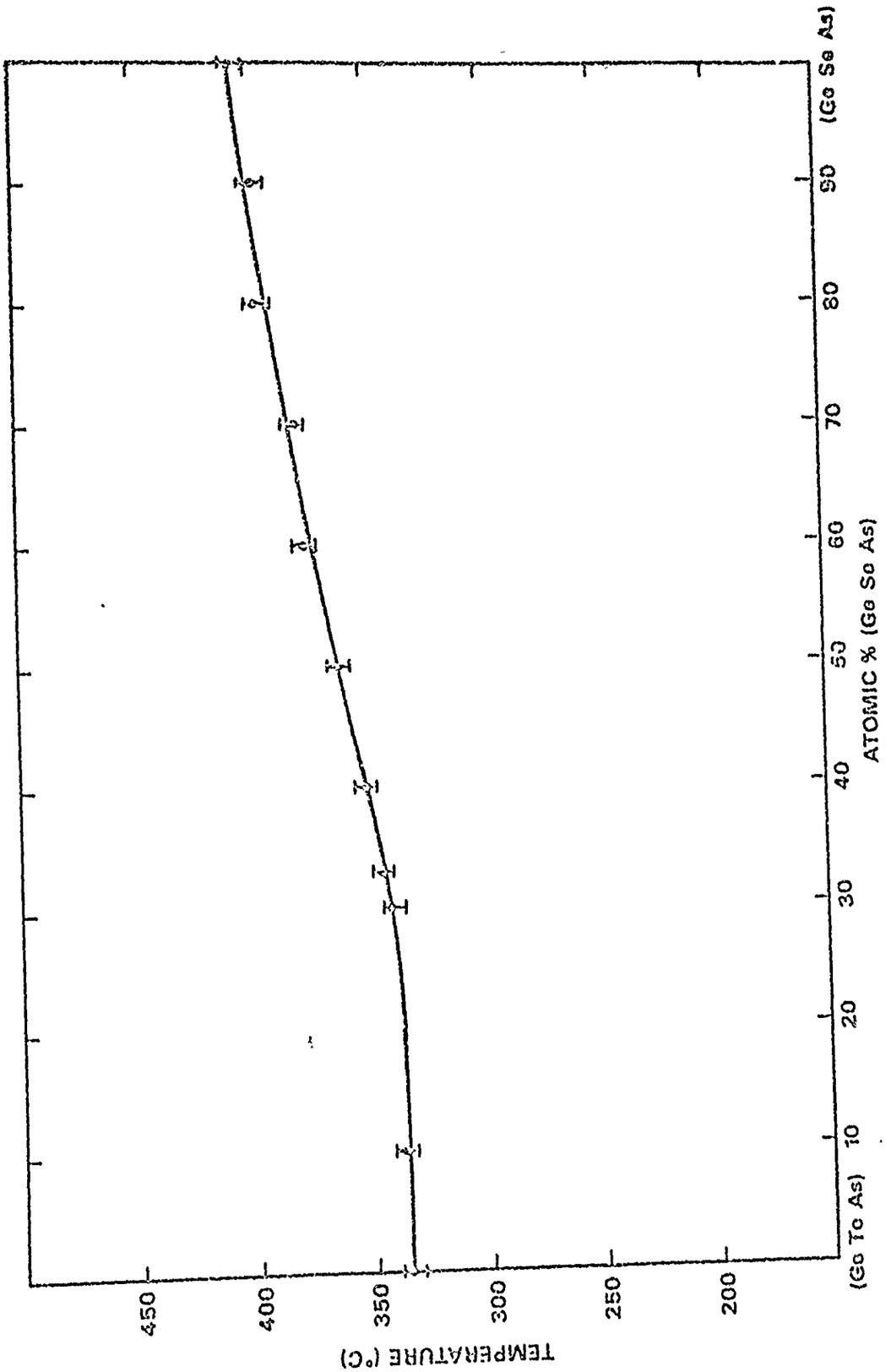
TEMPERATURE (°C)
450
400
350
300
250
200
(Ge Te As)
10
20
30
40
50
60
70
80
90
(Ge Se As)
ATOMIC % (Ge Se As)

composition, although we were, in fact, able to obtain such a glass by very rapid quenching of a small sample.

2.4.3 Conclusions

We have found the three-fold coordination model for predicting the highest values of T_g in multicomponent chalcogenide systems to be very effective. In particular, it helps to identify regions of glass formation which would not have been suspected by examination of the binary or ternary subsystems which bound the multicomponent system. Indeed we suspect that new glass systems may be discovered by conscientious application of this bonding model.

Questions of major importance still remain unanswered by our effort to sort o. . the possible behavior of T_g in multicomponent chalcogenide systems:

1. What is the correlation between T_g and band gap among the three-fold coordinated chalcogenide subsystems, and does this correlation constitute a limit on T_g at constant band gap?
2. Within the three-fold subsystems, what determines the optimum ratio of IV:V:VI components at maximum T_g ? Preliminary results from the SiTe-As and SiTe-GeTe-As systems indicates that the $IV_{40}V_{20}VI_{20}$ ratio approaches this optimum, but at present we have no good model to account for this correlation.
3. Finally, if the three-fold coordination model is to gain credibility, it will require structural confirmation via diffraction or other structural experiments which directly sample the nearest neighbor environment of each atom type.

3. ABSTRACTS OF COMPLETED WORK

3.1 Introduction

During this portion of the contractual period several studies initiated both during the last period and during the past several months have reached either the prepublication stage or have been published. Rather than continue to summarize this work we are simply including the abstracts from the preprints or reprints. These completed papers are available from ECD, a few copies of which are also included along with the report, and are listed in the appendices.

The papers cover those topics to which we have addressed our attention over the past year. They deal, for example, with structural activities in which the amorphous state in silicon and germanium is achieved in a variety of ways (including ion implantation performed at the Hughes Laboratories) which are then compared. The impact of defects and impurities is quite dramatic and these results enable us for the first time not only to sort out the impurity influences but also to obtain a reasonable estimate of the difference in impurity content among the various preparation schemes.

We also have a continuing interest in the marriage between the amorphous semiconductor technology and the more conventional solid-state electronics art. This involves a consideration of interfaces, contacts and electrodes and led directly to our study of Pd_2Si. In its own right this study represents a major contribution to the

understanding of an important silicon-electrode interaction.

Our long-standing involvement in materials characterization has been responsible for our collaboration with A. Bienenstock on the structure of the Te-based memory glasses. The elucidation of the crystallization behavior of these glasses is, of course, also part of our program, presented in the last report to ARPA and recently published. This abstract is included below as it represents completed work. We are currently maintaining our effort in understanding these crystallizing glasses as outlined earlier in this report.

The sputtering process by which most of the alloy glasses are prepared has in the past been mostly an uncharacterized facet of our work. This has sponsored our explorations of the argon content in sputtered films and of the desorption process. E. A. Fagen's first contribution to this program -- delivered also as a talk to the APS March meeting -- is included here.

And H. K. Rockstad's studies of transport and the switching process (and their interrelationship) in many of the same materials that we structurally characterize, is represented by completed work in these fields abstracted below along with E. A. Fagen's work on photoconductivity.

3.2 Structural Studies

3.2.1 "Structure and Electrical Characteristics of Epitaxial Palladium Silicide Contacts on Single Crystal Silicon and Diffused p-n Diodes" by W.D. Buckley and S.C. Moss (submitted to Solid-State Electronics).

Pd_2Si contacts to single crystal silicon have been made by depositing Pd at room temperature and annealing at a succession of elevated temperatures. The silicide so formed is a single crystal, even at room temperature. Its crystal structure is uniquely related to that of the underlying silicon with the basal plane of Pd_2Si making an excellent match, with respect to silicon atom positions, with the (111) plane of silicon. Understanding this epitaxy leads to an appreciation of the excellent electrical characteristics of these contacts which are shown to be superior to alloyed aluminum. For comparison, barrier height measurements reproduce earlier results of Kircher on Pd_2Si formed during a high temperature ($200^{\circ}C$) deposition of Pd.

3.2.2 "Impurity Effects on the Structure of Amorphous Silicon and Germanium Prepared in Various Ways" by S. C. Moss, P. Flynn and L. - O. Bauer (submitted to Phil. Mag.).

Thin film transmission electron diffraction patterns from amorphous silicon, prepared by ion-implantation, RF sputtering and vapor deposition (evaporated) are strikingly similar in most details except in the exact position of the diffuse peaks. For high purity silicon, either evaporated or ion-implanted, the first diffuse ring, for example, comes consistently at a value of $s = 4\pi\sin\theta/\lambda$, slightly lower than the (111) Bragg

peak of the crystallized film. For sputtered films this sequence is reversed both in electron diffraction and in X-ray scattering from thick films of ~ 8μ . The reversal is attributed to impurities, most probably oxygen or nitrogen. The implications for structural analysis are presented in terms of the derivation of positions and shapes of the peaks in the pair correlation function. This structural information is qualitatively invoked to explain some observations on properties. The entire effect seems somewhat less pronounced in amorphous germanium films of all thicknesses, although it anneals out much more readily in germanium than in silicon.

3.2.3 "Neutron and X-ray Diffraction Radial Distribution Studies of Amorphous $Ge_{.17}Te_{.83}$" by F. Betts, A. Bienenstock, D.T. Keating, and J. deNeufville (In press, J. Non-Crystalline Solids).

Bulk amorphous samples of amorphous $Ge_{.17}Te_{.83}$ have been prepared by quenching of small molten droplets. Radial distribution functions have been constructed from both x-ray and neutron diffraction intensity data. These indicate first neighbor peaks at 2.75 Å and 2.65 Å, respectively, indicating the greater sensitivity of the neutron RDF to atoms pairs containing the smaller Ge atom. The first peak area in both RDF's is not consistent with twofold coordination of

the Ge. It can be fit by two types of models. In the first, the Ge is fourfold and the Te two fold coordinated. In the second, the Ge is threefold coordinated, while some Te are threefold and others twofold coordinated. It is shown that both types of models are consistent with RDF's performed on other compositions.

3.3 Thermal Analysis of Materials

3.3.1 "Thermally Stimulated Argon Release from Amorphous Alloy Films" by E. A. Fagen, Mat. Res. Bull. 7, 279, (1972).

A new diagnostic technique is described for the study of kinetic processes in sputtered thin films. Examples are given of application to amorphous chalcogenide alloys, and are compared with the results of differential scanning calorimetry.

3.3.2 "Thermal Crystallization of Selected Thin Films of Te-Based Memory Glasses" by S. C. Moss and J. P. deNeufville, Mat. Res. Bull. 7, 423 (1972).

X-ray diffraction on 1 - 10 μ films and transmission electron microscopy and diffraction on ~ 500 Å films have been performed on sputtered glasses based on the Ge-Te eutectic at $Ge_{15}Te_{85}$. The rates and morphologies of crystallization have been studied along with the influence of selected impurities. Thermodynamic factors have also been considered all of which

has contributed to our understanding of the memory setting action in the RM-256 computer memory array. It appears that this memory effect is due to the fine scale crystallization of Te dendrites and that the supression of the telluride formation may play an important role.

3.4 Theortical Studies in Transport and Switching

3.4.1 "Comments on the ac Conductivity of Amorphous Chalcogenides" by H. K. Rockstad, Solid State Comm., 9, 2233 (1971).

The comparison of the ac conductivity for various amorphous chalcogenides with band gaps ranging from less than 1 to greater than 2 eV is discussed in terms of localized states. Comments in the literature concerning curious results in the ac conductivity are discussed and an interpretation given.

3.4.2 "Electrical Stability of Bulk S-Shaped Negative Differential Conductivity Media" by H. K. Rockstad and M. P. Shaw, submitted for publication in Applied Physics Letters.

As originally postulated by Ridley, bulk media exhibiting isothermal current controlled negative differential conductivity (NDC) are shown to be unstable with respect to small fluctuations in the current density, leading to current density filamentation. In contrast to Ridley's arguments, however, we describe and

elucidate the instability in terms of internal induced magnetic flux. We show that Lenz's law does not apply to NDC points.

3.4.3 "Analysis of Photoconductivity in Amorphous Chalcogenides" by T.C. Arnoldussen, R. H. Bube, E. A. Fagen and S. Holmberg, J. Appl. Phys. 43, 4 (1972).

Starting with standard semiconductor recombination statistics and a generalized distribution of localized states within the mobility gap of an amorphous semiconductor, a model for photoconductivity has been developed. Consistency with experimentation phenomena requires the inclusion in this model not only of the traditional nonlocalized-to-localized state recombination transitions, but also of two types of localized-to-localized state recombination transitions: (1) from states nearer than a critical energy to the conduction edge, to similar states nearer than a critical energy to the valence edge; (2) from states near the mobility edges to states near the the thermal equilibrium Fermi level. Such a model has general applicability to a variety of different types of amorphous chalcogenides, encompasses previously reported variations of photoconductivity with intensity and temperature, and provides a way of estimating the characteristic parameters of localized states in those materials. Quantitative application of the model is made to photoconductivity data for three amorphous chalcogenides.

4. LIST OF CONTRIBUTORS

The present report represents a significant departure from the two earlier reports in that the materials survey results are now organized in terms of chemistry rather than in terms of experimental technique. We feel that an important advance has occurred when the overlap of such disparate studies as thermopower and calorimetry, transport and electron microscopy, can be focused on the same group of materials to yield, with the help of a simple conceptual model, an overview of many of the chalcogenide glass properties. We have begun to find answers to the basic concerns which underly all these studies: the detailed atomic and electronic structures, their interrelationship, and their role in controlling the physical and chemical properties of the chalcogenide glasses.

In a highly cooperative and integrated program of this sort it is sometimes difficult to identify the roles of the individual scientists. The traditional technique-oriented specialization of individual scientists occurs to some extent at ECD, and the contribution of each man can be superficially correlated with his current area of specialization: J. P. deNeufville, calorimetry and sputtering; E. A. Fagen, photoconductivity and mass spectrometry; S. C. Moss, diffraction and microscopy; H. K. Rockstad, thermoelectric power and conductivity. While the data inevitably flow from specific experiments traceable to specific individuals, most of the resulting overview of past progress and motivation towards new research emerges as equally shared common ground.

SCIENTISTS

J. P. deNeufville

E. A. Fagen

S. C. Moss

H. K. Rockstad

TECHNICIANS

Ingot and cathode fabrication

J. Tyler

Calorimetry and sputtering

D. Sarrach

Conductivity and optical absorption

R. Séguin

Thermopower and conductivity

R. Flasck

X-ray diffraction

R. Goss

Electron microscopy and diffraction

P. K. Flynn

Photoconductivity and argon desorption

R. Shaw

5. REFERENCES

1. First Semi-Annual Technical Report, Contract DAHC15-70-C-0187, Advanced Research Projects Agency, Washington, D. C. (1970).

2. Second Semi-Annual Technical Report, Contract DAHC15-70-C-0187, Advanced Research Projects Agency, Washington, D. C. (1971).

3. J. P. deNeufville, J. Non-Crystalline Solids, 8/9, 85 (1972) (in press).

4. E. A. Fagen, Mat. Res. Bull. , 279 (1972).

5. D. Turnbull, in Physics of Non-Crystalline Solids (edited by J. W. Prins) (Amsterdam: North Holland) pp. 41-51 (1965).

6. H. S. Chen and D. Turnbull, J. Appl. Phys. 40, 4214 (1969).

7. J. P. deNeufville and D. Turnbull, Discussions of the Faraday Society, No. 50, 182 (1970).

8. T. Takamori and R. Roy, Talk presented at the Fall Meeting, American Ceramic Society Meeting, Bedford Springs, Pa., October, 1971.

9. F. Betts, A. Bienenstock, D. Keating and J. deNeufville, J. Non-Crystalline Solids (in press); F. Betts, A. Bienenstock and S.R. Ovshinsky, J. Non-Crystalline Solids 4, 554 (1970); Ibid. 2, 347 (1970).

10. G. Fisher, J. Non-Crystalline Solids 8/9 (1972) (in press).

11. S. K. Bahl and K. L. Chopra, J. Appl. Phys. 41, 2196 (1970).

12. R. Messier and R. Roy, Mat. Res. Bull. 6, 749 (1971).

13. W. E. Howard and R. Tsu, Phys. Rev. B 1, 4709 (1970).

14. D. E. Polk, J. Non-Crystalline Solids 5, 365 (1971).

15. N. Shevchik and W. Paul, J. Non-Crystalline Solids 8/9 (1972) (in press).

16. D. Turnbull, Contemp. Phys. 10, 473 (1969).

17. S. C. Moss and J. P. deNeufville, Mat. Res. Bull. 7, 423 (1972).

18. H. K. Rockstad, S. Iwasa and R. Flasck, J. Non-Crystalline Solids, 8/9 (1972) (in press).

19. A. Rose, Concepts in Photoconductivity and Allied Problems, (Interscience Publishers, N. Y., 1963).

References - cont'd.

20. H. K. Rockstad, J. Non-Crystalline Solids, 2, 224 (1970).

21. R. M. Hill, Phil. Mag. 23, 59 (1971).

22. J. W. Osmun and H. Fritzsche, Appl. Phys. Letters 16, 87 (1970).

23. T. Arnoldussen, R. H. Bube, E. A. Fagen and S. Holmberg, J. Appl. Phys. 43, 1798 (1972).

24. M. H. Cohen, H. Fritzsche and S. R. Ovshinsky, Phys. Rev. Letters 22, 1065 (1969).

25. S. C. Moss and J. F. Graczyk, Phys. Rev. Letters 23, 581 (1969); M. L. Theye, Mat. Res. Bull. 6, 103 (1971); F. L. Galeener, Phys. Rev. Letters 27, 421 (1971); M. H. Brodsky, R. S. Title, K. Weiser and G. D. Pettit, Phys. Rev. B 1, 2632 (1970).

26. M. Aven and J. S. Prener, Physics and Chemistry of II-VI Compounds, (Interscience, New York, 1967) Chapter 4.

27. Y. Kawamoto and S. Tsuchihashi, J. Amer. Ceram. Soc. 54, 131 (1971).

28. H. Krebs and P. Fischer, in Discussions of the Faraday Society No. 50 (1970).

29. A. Ray Hilton, C. E. Jones and M. Brau, Infrared Physics 4, 213 (1964).

30. N. Kh. Abrikosov, V. F. Bankina, L. V. Poretskaya, L. E. Shelimova and E. V. Skudnova, Semiconducting II-VI, IV-VI, and V-VI Compounds, Plenum Press, New York, 1969).

APPENDIX I

Reprints accompanying this report

1. H. K. Rockstad, "Comments on the ac Conductivity of Amorphous Chalcogenides", Solid State Comm., 9, 2233 (1971).

2. E. A. Fagen, Thermally Stimulated Argon Release from Amorphous Alloy Films", Mat. Res. Bull. 7, 279 (1972).

3. T. C. Arnoldussen, R. H. Bube, E. A. Fagen and S. Holmberg, "Analysis of Photoconductivity in Amorphous Chalcogenides", J. Appl. Phys. 43, 4 (1972).

4. S. C. Moss and J. P. deNeufville, "Thermal Crystallization of Selected Thin Films of Te-Based Memory Glasses", Mat. Res. Bull. 7, 423 (1972).

APPENDIX II

Preprints accompanying this report:

1. W. D. Buckley and S. C. Moss, "Structure and Electrical Characteristics of Epitaxial Palladium Silicide Contacts on Single Crystal Silicon and Diffused p-n Dioded".

2. S. C. Moss, P. Flynn and L. -O. Bauer, "Impurity Effects on the Structure of Amorphous Silicon and Germanium Prepared in Various Ways".

3. F. Betts, A. Bienenstock, D. T. Keating, and J. deNeufville, "Neutron and X-ray Diffraction Radial Distribution Studies of Amorphous $Ge_{.17}Te_{.83}$".

APPENDIX III

Talks presented by ECD research staff members on work supported by ARPA:

J. P. deNeufville

1. Fall Colloquium - Materials Science Department, Case-Western Research University, 1971.
2. Contributed Paper - Annual Meeting Am. Ceramic Soc., Wash., D. C. May (1972).

E. A. Fagen

1. Contributed paper, March meeting APS, Atlantic City (1972).

S. C. Moss

1. Invited Talk - Thin Film Div. AVS Boston, Nov. 1971.
2. Invited Talk - IBM Watson Research Labs., April 1972.
3. Physics Colloquium, Michigan State University, Oct. 1971.
4. Engineering Sciences Colloquium, Brown University, Nov. 1971.
5. Materials Science Colloquium, Lehigh University, Dec. 1971.
6. Physics Colloquium, Oakland University, Jan. 1972.
7. Materials Center Colloquium, Univ. of Maryland, Feb. 1972.
8. Physics Colloquium, University of Houston, March, 1972.
9. Contributed Paper, Winter Meeting APS, Boston (1971).

H. K. Rockstad

1. Contributed Paper, Annual Meeting APS, San Francisco (1972).

2. Contributed Paper, March Meeting APS, Atlantic City (1972).